

ISSN: 0028-8306

## A revised paleoseismological record of late Holocene ruptures on the Kekerengu Fault following the 2016 Kaikōura earthquake

Philippa Morris, Timothy Little, Russ Van Dissen, Mark Hemphill-Haley, Jesse Kearsse, Matthew Hill, Jessie Vermeer & Kevin Norton

To cite this article: Philippa Morris, Timothy Little, Russ Van Dissen, Mark Hemphill-Haley, Jesse Kearsse, Matthew Hill, Jessie Vermeer & Kevin Norton (2022): A revised paleoseismological record of late Holocene ruptures on the Kekerengu Fault following the 2016 Kaikōura earthquake, New Zealand Journal of Geology and Geophysics, DOI: [10.1080/00288306.2022.2059766](https://doi.org/10.1080/00288306.2022.2059766)

To link to this article: <https://doi.org/10.1080/00288306.2022.2059766>



Published online: 20 Apr 2022.



Submit your article to this journal [↗](#)

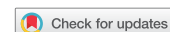


View related articles [↗](#)



View Crossmark data [↗](#)

RESEARCH ARTICLE



## A revised paleoseismological record of late Holocene ruptures on the Kekerengu Fault following the 2016 Kaikōura earthquake

Philippa Morris <sup>a</sup>, Timothy Little <sup>a</sup>, Russ Van Dissen <sup>b</sup>, Mark Hemphill-Haley<sup>c</sup>, Jesse Kearsse<sup>a</sup>, Matthew Hill <sup>b</sup>, Jessie Vermeer <sup>d</sup> and Kevin Norton <sup>a</sup>

<sup>a</sup>School of Geography, Environment and Earth Sciences, Victoria University of Wellington, Wellington, New Zealand; <sup>b</sup>GNS Science, Lower Hutt, New Zealand; <sup>c</sup>Department of Geology, Humboldt State University, Arcata, CA, USA; <sup>d</sup>School of Geography, Earth and Atmospheric Sciences, The University of Melbourne, Parkville, Australia

### ABSTRACT

The  $M_w$  7.8 Kaikōura earthquake of November 14th, 2016 provided rare opportunities to evaluate ground deformation during a large strike-slip earthquake. Following the earthquake, both halves of a displaced paleoseismic trench were re-excavated and extended to test, refine, and extend the known late Holocene chronology of surface rupturing earthquakes on the Kekerengu Fault. 28 organic-bearing samples were collected during these excavations. Of these, six samples provided new  $^{14}\text{C}$  ages that could be superimposed on the preferred age model of (Little VDR, Kearsse J, Norton K, Benson A, Wang N. 2018. Kekerengu fault, New Zealand: Timing and size of Late Holocene surface ruptures. *Bulletin of the Seismological Society of America*. 108(3B):1556–1572) to derive an expanded, updated age model of earthquake events on the fault that is now based on 16 dated samples. Including the 2016 earthquake, we recognise six surface rupturing earthquakes on the Kekerengu Fault since ~2000 cal. B.P. Based on the last five events, our analysis yields an updated estimate of the mean recurrence interval for surface rupturing on the fault of  $375 \pm 32$  yrs ( $1\sigma$ ) since ~1650 cal. B.P. An older, sixth event (E5) was not included in the preferred age model due to uncertainties in interpretation; however, incorporating this event into an alternative, six-event age model would adjust the recurrence interval estimate to  $433 \pm 22$  yrs ( $1\sigma$ ) since ~2000 cal. B.P.

### ARTICLE HISTORY

Received 25 November 2021  
Accepted 25 March 2022

### HANDLING EDITOR

Andy Nicol

### KEYWORDS

Paleoseismology; structural geology; strike-slip faults; 2016 Kaikōura earthquake; multi-fault rupture

## Introduction

The  $M_w$  7.8 Kaikōura earthquake of the 14th of November 2016 ruptured ~20 faults in the Marlborough Fault System (MFS) over a length of ~180 km, in an unusually complex, multi-fault rupture sequence (Figure 1) (Hamling et al. 2017; Litchfield et al. 2018; Mouslopoulou et al. 2019). The fault with the largest surface displacement during this earthquake was the NE-SW striking Kekerengu Fault, which accommodated >8 m of dextral slip along much of its length, and locally reached a slip of ~12 m. This slip value is among the five largest coseismic surface displacements recorded globally to date (Kearsse et al. 2018; Little et al. 2018). In January 2016, approximately 10 months prior to this earthquake, three paleoseismological trenches had been excavated across the north-eastern part of the Kekerengu Fault near the coast (Figure 2). Little et al. (2018) used a suite of 10 radiocarbon samples from these trenches to model the timing of three late Holocene surface-rupturing paleoearthquakes since ~1250 cal. B.P. Statistical analysis of these paleoearthquakes and the 2016 rupture yielded an estimate for the mean recurrence interval for surface rupturing on this part of the fault of  $376 \pm 32$  yrs ( $1\sigma$ ). Combined with the observed  $9.0 \pm$

0.1 m of single-event displacement (SED) in 2016 on the trenched part of the fault (Kearsse et al. 2018), and assigning a coefficient of variation of 0.5 to this estimate of mean SED, Little et al. (2018) inferred a mean late Holocene dextral-slip rate of  $24 \pm 12$  mm/yr ( $1\sigma$ ) for the eastern Kekerengu Fault. The three paleoearthquakes identified by Little et al. (2018) were dated at 249–108, 528–356, and 1249–903 cal. yrs B.P. respectively. They also suggested that a fourth, older paleoearthquake occurred either 1) at >1605 cal. B.P. or 2) in the interval 1673–1205 cal. yrs B.P. This ambiguity in the age of the oldest event arose from uncertainties in stratigraphic interpretation of radiocarbon ages of detrital charcoal in the infill of a coseismic fissure deposit, an ambiguity which the authors did not attempt to resolve in that paper.

In this paper, we update and revise the paleoseismic chronology for the Kekerengu Fault established by Little et al. (2018) based on new stratigraphic data and  $^{14}\text{C}$  ages collected in the same study area. Approximately 15 months after the 2016 earthquake (February 2018), the fragmented (unequal) halves of Trench 1 of Little et al. (2018) were re-excavated as part of a study comparing equivalent pre- and post-earthquake trench logs in order to identify

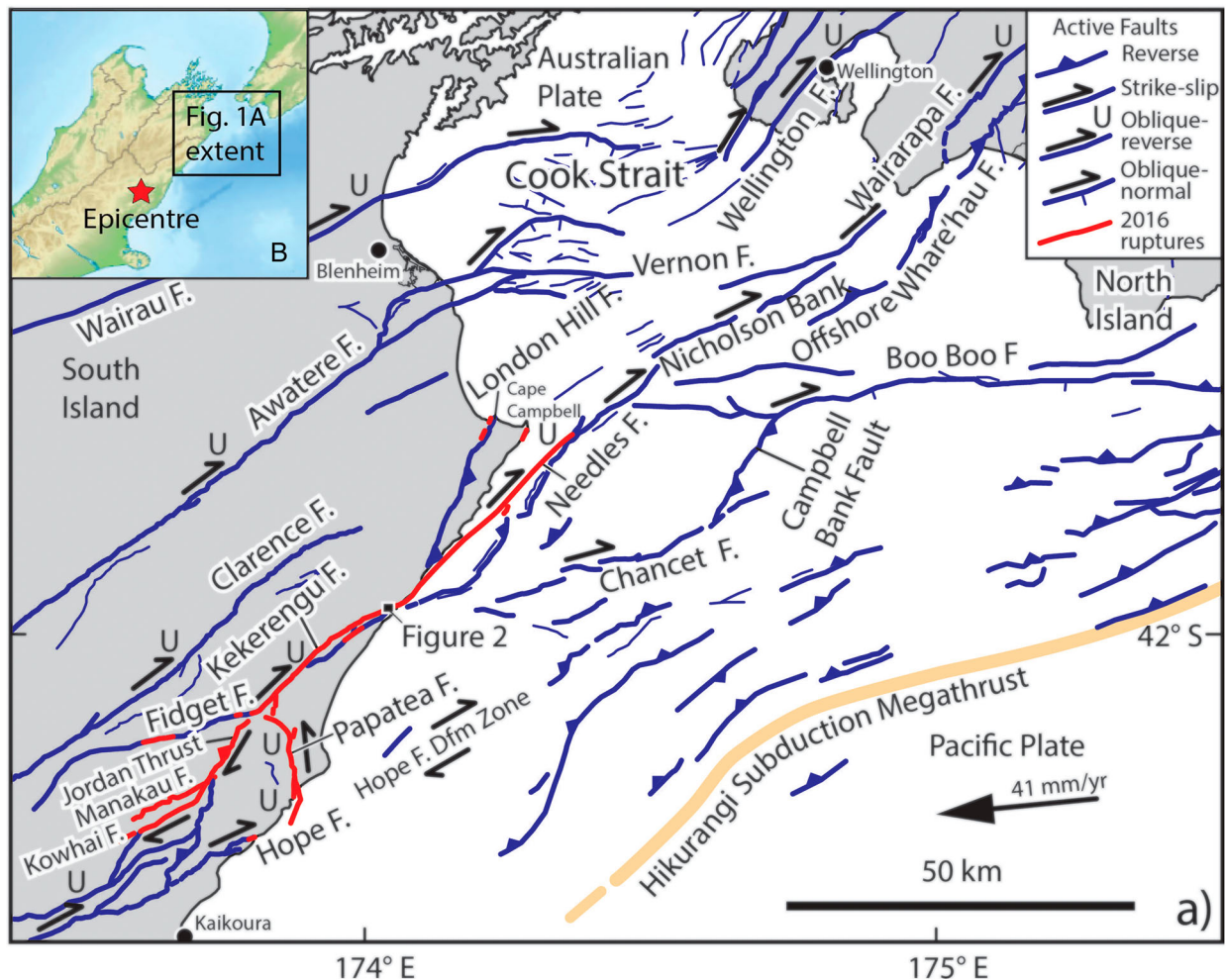


**Figure 1. A,** Tectonic map of the Cook Strait region between the North and South Island of New Zealand, encompassing the northern grouping of faults, including the Kekerengu Fault, that ruptured in the 2016 Kaikōura earthquake (red lines, Litchfield et al., 2018). Active faults that did not rupture in 2016 are shown in blue (Barnes et al., 2008). Epicentre location for the 2016 earthquake (shown in **B**) is from Nicol et al. (2018). Figure adapted from Little et al., 2018.

and evaluate the incremental deformation that accumulated in 2016 as a result of a single, ~9 m strike-slip rupture (Morris et al. 2021). In addition to exhuming the old trench walls, the following new excavations were made: 1) an entirely new trench, ‘Trench 4’, was excavated across the 2016 ground deformation zone (including a moletrack) adjacent to the Trench 1 (T1) fragments; and 2) the displaced fragments of T1, after exhuming, were extended several metres across the fault zone to encounter material that had been laterally translated into place during the 2016 earthquake (and hence, not previously logged). Finally, we made field observations of earthquake fissures that had opened up during the Kaikōura earthquake, in particular noting the rate and process by which they were being infilled in the post-seismic period. Several samples of charcoal were collected from one of the deepest of these fissures, a fault-bounded opening that had demonstrably ruptured and been infilled during an earlier earthquake before being opened again in 2016. In total, 18  $^{14}\text{C}$  ages were derived from the samples collected in the post-earthquake excavations,

the results and implications of which are reported in this paper.

Our new synthesis of paleoseismicity on the Kekerengu Fault embraces at least one additional (older) paleoearthquake than was recognised by Little et al. (2018), thus allowing us to calculate a revised estimate of mean Recurrence Interval (RI) that is based on the last five surface rupturing events (rather than four). These new results provide important information about the timing and size of surface rupturing earthquakes on the fault and will be useful for future evaluation and modelling of seismic hazard in central New Zealand. In addition, this well constrained, detailed chronology of late Holocene surface ruptures on the eastern part of the Kekerengu Fault may prove valuable for future studies that aim to understand the seismic behaviour of the MFS as a whole; for example, comparative studies exploring the possibility that other multi-fault rupturing earthquakes have involved the Kekerengu Fault prior to 2016 (Langridge *et al.*, this issue), or that earthquakes closely spaced in time have been triggered as a result of stress interactions between the Kekerengu Fault and nearby structures

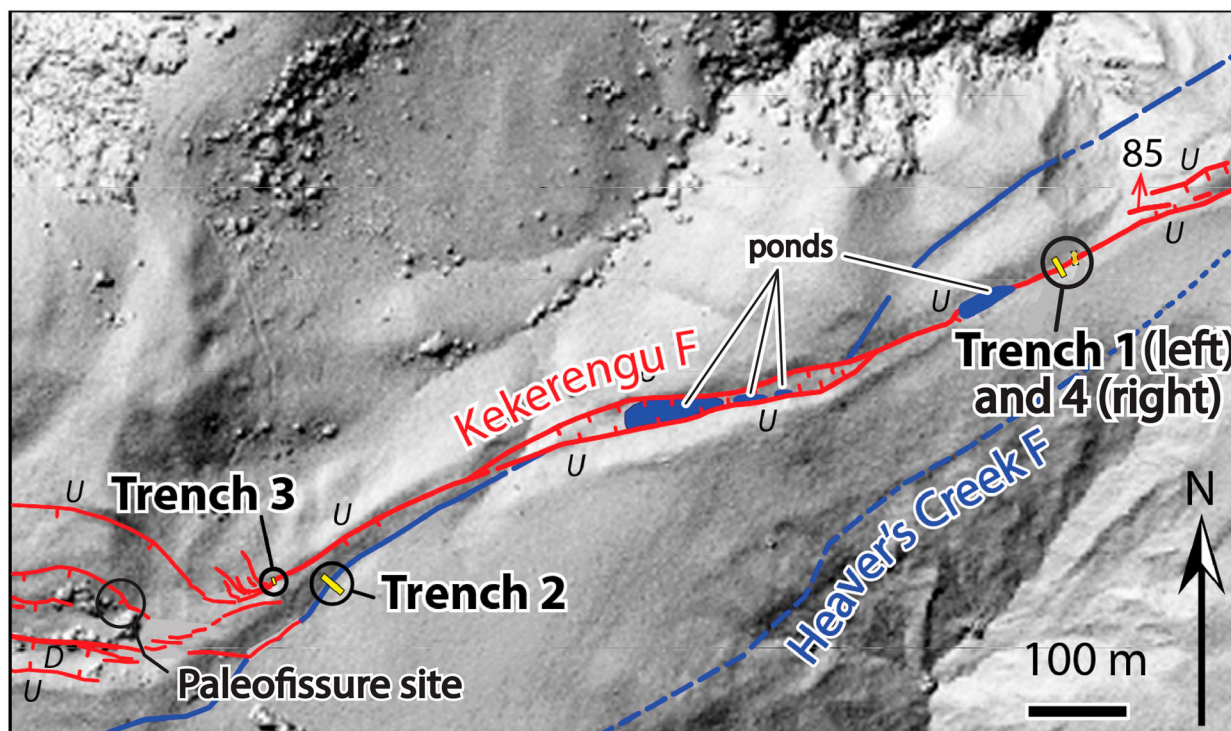


**Figure 2.** Map of fault traces near the three paleoseismic trenches excavated in January 2016 (Trenches T1, T2 & T3; adapted from Little et al. 2018), the paleofissure site to the southwest (see also Figure 5), and Trench 4 excavated in 2018 (dashed) adjacent to the dismembered portions of Trench T1 (see also Figure 4). Red traces show faults strands that ruptured in the 2016 earthquake, while blue traces show fault strands that did not rupture in 2016. See Figure 1 for location. Background shaded DSM derived from analysis of 2014–2015 LINZ aerial imagery, gridded at 1 m (Hill and Ashraf 2017).

to the south and north – such as the Hope and Wairarapa Faults respectively (Little et al. 2018).

A necessary first step in any such research is the construction of robust and precise earthquake chronologies for each of the key faults. Understanding how the faults of the MFS may (or may not) interact with one another is important for determining local and regional seismic hazard, and crucial to understanding the nature and distribution of the Pacific-Australian plate boundary deformation through central New Zealand. The Kekerengu Fault is an important source of local and regional seismic hazard, and the implications of the tempo and activity on the fault are far-reaching (including the Wellington region).

## Background

The active faults of the MFS (Figure 1) are located in the northeast section of the South Island of New Zealand, where they have accommodated relative motion between the Pacific and Australian plates for at least the past ~7 Ma (Little and Jones 1998). The MFS consists of a series of NE-striking, dextral to dextral-reverse faults (uplifted on their NW sides) that transfer motion from the Alpine Fault to the SW, into the upper plate of the Hikurangi Subduction margin, to the NE. Some of this motion traverses the Cook Strait to link with the NNE-striking dextral slip faults of the

North Island Dextral Fault Belt, including the Wellington and Wairarapa Faults.

The Kekerengu Fault typically strikes 060–070° and dips 60–80°, predominantly to the NW (Kearse et al. 2018; Little et al. 2021). At its SW end, it transfers slip northward from the Hope Fault via the intervening Jordan Thrust and adjacent fault splays, such as the Upper Kowhai and Manakau Faults. The Hope Fault is the most active fault in the MFS and is segmented; the eastern central Conway segment has an inferred average dextral slip rate of ~15 mm/yr (since 14 ka, Hatem et al. 2020), to  $23 \pm 4$  mm/yr (Langridge et al. 2003). The NE end of the Kekerengu Fault continues offshore (where it is referred to as the Needles Fault) and extends northward towards the Cook Strait.

About ten months prior to the Kaikōura earthquake, three paleoseismic trenches were excavated across the Kekerengu Fault in January 2016 (Figure 2). They were located about 2 km west of the coast on rolling hills near the inferred intersection of the Kekerengu Fault with its southern dextral-slip splay, the Heaver's Creek Fault (Figure 2). The Heaver's Creek Fault ruptured in 2016 along a short segment (< 3 km) with a small amount of dextral ground surface displacement (< 30 cm) (Kearse et al. 2018). The trenches were dug on a section of the main Kekerengu Fault that strikes ~5° more easterly than the average strike of the fault (~070) to the west. As expected for that strike, this near-coastal strand has accrued a

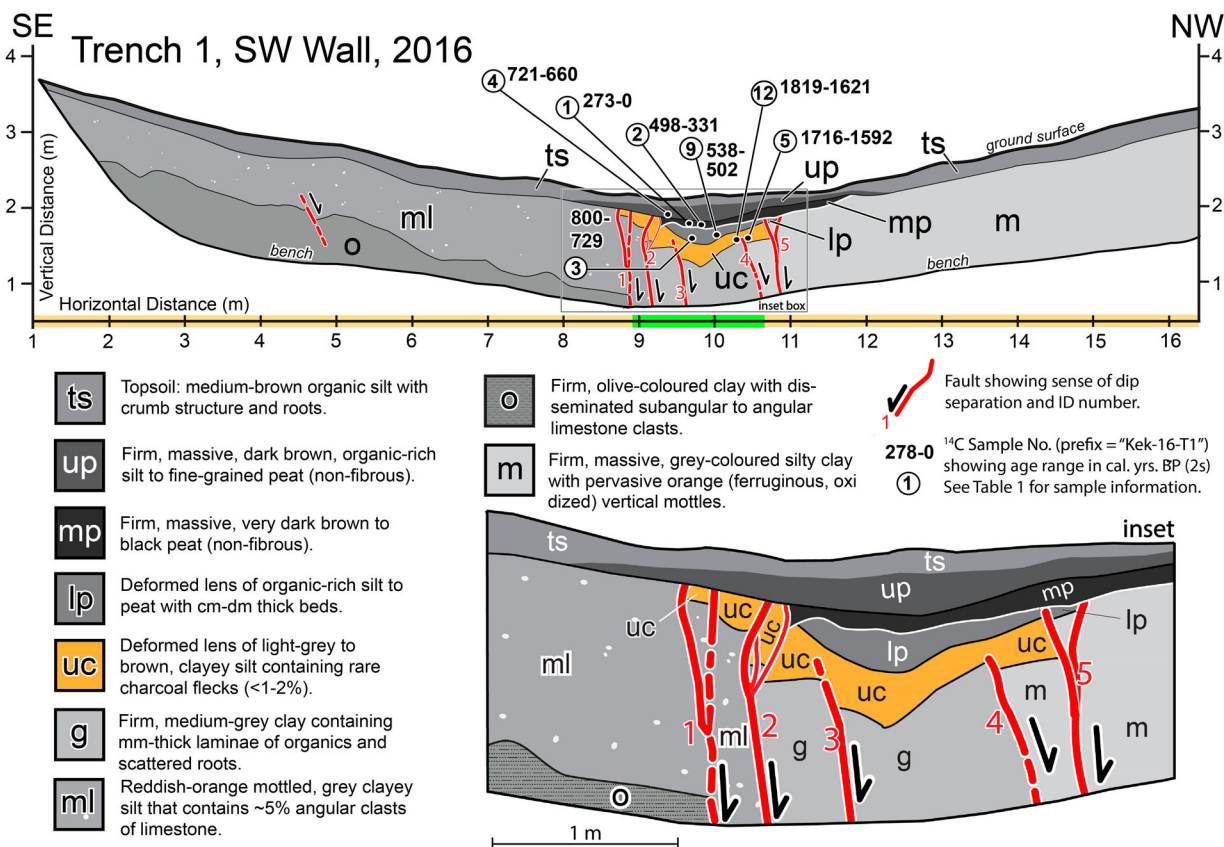


**Figure 3.** Pre-earthquake log of the southwest (SW) wall of Trench T1 (adapted from Little et al. 2018), showing numbered faults and basic stratigraphy. Only the top part of the trench is shown here (down to the bench), as this is the depth to which the trench was re-excavated in 2018. The northwestern end of the original trench log is also clipped, as it is not relevant to the current study.  $^{14}\text{C}$  age ranges are quoted in cal. yrs B.P. at 95% confidence. For more information on the  $^{14}\text{C}$  samples, see Table 2. No vertical exaggeration. Orange highlight along the scale bar below the trench log identifies the horizontal extent of material that was logged in the corresponding post-earthquake trenches (see Figure 4, Figures 6–8). Green bar underneath the central part of the log represents the future location of the highly deformed central part of the 2016 rupture zone. Inset (labelled) shows an enlarged version of this (future) central rupture zone (see box on the main figure) so that detailed stratigraphic relationships can be more easily identified and compared with post-earthquake trench exposures.

transtensional dextral-slip in the long-term, as manifested by a string of small sediment-filled pull-apart basins bounded by oblique-normal faults on one or both of their margins (Little et al. 2018), and by a reversal in the net sense of throw across the fault (transitioning from up-to-the-NW farther inland to down-to-the-NW near the coast). The three trenches were dug across linear fault depressions interpreted as transtensional fault furrows. Trench 1 was the farthest east of the three, and was excavated ~100 m to the east of a fault-bounded sag pond. This trench was aligned at right angles to a swampy, 2–3 m deep fault furrow (Figure 2). Although the NE wall of the trench collapsed prior to logging, it had been cleaned and photographed. The SW trench wall was scraped, cleaned, gridded, photographed, flagged and logged at a scale of 1:20; then it was backfilled, smoothed over, and replanted with grass. During the Kaikōura earthquake, T1 was split in half by the rupture with the two fragments of the trench being displaced dextrally by ~9 m (Little et al. 2018; Morris et al. 2021).

Differences in the density of grass cover as a result of backfilling and reseeded made the old trench margins easy to re-identify months after the earthquake. Although displacement initially appeared to be a discrete offset along a single linear fault trace, detailed analysis indicates that some of the strike-slip deformation was distributed across a central rupture zone >1.5 m wide (Figure 3). Slip across this complexly deformed zone was in part accommodated by: a) vertical-axis rotation of elongate, fault-bounded blocks of near-surface sediment and soil; and b) pervasive shearing of soft sediment between closely spaced faults strands (Little et al. 2021; Morris et al. 2021). One effect of these distributed types of deformation in the rupture zone was to cause a change in the stratigraphic thickness, shape, and/or ordering of units as observed on the pre- vs. post-earthquake versions of the same trench wall. As argued by Morris et al. (2021), these changes were caused by the out-of-plane nature of the distributed strike-slip shearing and rotation relative to the (exhumed) trench wall.

**Table 1.** Summary table of evidence for paleo-events E1, E2 and E3 in Trench 1 of Little et al. (2018); pre-earthquake evidence for each paleo-event is shown in the first column, while each remaining column details the evidence for these same paleo-events on the respective post-earthquake trench walls. Boxes shaded green indicate that the evidence for a given paleo-event is still identifiable, while boxes shaded orange indicate that event evidence is no longer observed (because it was destroyed or changed in the 2016 earthquake).

	Event evidence from 2016 Trench 1, SW wall	Trench S1, SW wall	Trench S1, NE wall	Trench N1, SW wall
<b>Event E1</b>	Unit <i>mp</i> displaced, tilted Unit <i>up</i> unfaulted Slip on fault 2	Evidence destroyed by a reactivation of slip on fault 1 in 2016	Evidence destroyed in 2016	Evidence destroyed in 2016
<b>Event E2</b>	Unit <i>lp</i> displaced, tilted Unit <i>mp</i> unfaulted Slip on fault 5	Displacement observed on fault 2 -tilting of unit <i>lp</i> just NW of fault 2 creates angular unconformity between units <i>lp</i> and <i>mp</i> Still observed	Displacement and tilting observed on fault c Still observed	Steeper dip of <i>lp</i> in comparison to <i>mp</i> observed Destroyed by slip on fault 4, which caused lateral motion and shearing Fault 5 identified on this trench wall
<b>Event E3</b>	Base of unit <i>uc</i> displaced Unit <i>lp</i> unfaulted Slip on fault 3 and 4	Observed on fault 3 Observed on fault 5 Slip on fault 4 reactivated in 2016, destroying original offset observations (but slip on fault 3 still preserved)	Still observed on fault d Faults 3 and 4 not identified on this trench wall	Basal contact of unit <i>uc</i> still dips more steeply than <i>lp</i> (adjacent to fault 4) Relationship destroyed by slip on fault 4 in 2016 Fault 4 reactivated, destroying original offset observations. Fault 3 not recognised on this trench wall

Note: the dip of the basal contact of the unit *uc* also steepened with each paleoearthquake.

For example, buckling and folding of the pre-earthquake stratigraphy caused by the transcurrent deformation generated a ~1 m high compressional mound or ‘moletrack’ at the site, the amplitude and geometry of which varied laterally along strike.

### Pre-earthquake stratigraphy and cross-cutting relationships (January 2016)

#### Trench 1, southwest wall (refer to Figure 3)

The fault furrow transected by Trench 1 of Little et al. (2018) contained several lenses of organic-rich sediment. Depending on the lens and its location, they are variably either cut by a fault strand (these are labelled 1-5) or deposited across the upward termination of a fault strand without being offset (Figure 3). The lenses (units *uc*, *lp*, *mp* and *up*) were deposited in a swamp or shallow pond that developed in the central ~2 m of the fault furrow within a metre of the ground surface. On some of the fault strands, gently NE-plunging slickenlines were observed, indicating dextral-normal slip. The cross-cutting relationships observed in this trench allowed three paleoearthquakes to be identified by Little et al. (2018) – E1, E2 and E3. The evidence for each of these events is summarised in Table 1, and the radiocarbon results from this trenching are reported in Table 2.

The oldest of these events, E3, caused slip on faults 3 and 4, offsetting the base of the *uc* unit but not cutting the overlying peat, unit *lp* (Figure 3). From this, it was inferred that samples 5 (NZA 61217) and 12 (NZA 61218) predated E3, while samples 3 (NZA 61010) and 9 (NZA 61012) post-dated it. This gave a bracketed

age of 1716–729 cal. yrs B.P. for E3. The next youngest paleoseismic event, E2, caused slip on fault 5, which displaced the peat unit *lp*. The overlying peat (unit *mp*) is not cut by fault 5, and so samples 1 (NZA 61005) and 2 (NZA 61009) must postdate E2, whereas samples 3 and 9 pre-date it, bracketing E2 between 538–331 cal. yrs B.P. During the youngest paleoseismic event, E1, fault 2 displaced the unit *mp*; however, the overlying peat unit, *up*, was not displaced in this event as it overlaps faults 1 and 2. Therefore E2 is inferred to postdate sample 1 ( $^{14}\text{C}$  age for *mp* unit of 273–0 cal. yrs. B. P.). Sample 4 (NZA 61011) from the unfaulted unit *up* higher up the section yielded an anomalously old age (721–660 cal. yrs B. P.) that is older than  $^{14}\text{C}$  ages stratigraphically below it, and so was rejected as a depositional age. On this basis, E1 was interpreted to have taken place at <273 cal. yrs B.P.

Further confirmation of this sequence of earthquakes is provided by the incremental way in which the central syncline deepened. With each paleoearthquake, the dip of the syncline’s limbs progressively steepened, and the syncline tightened. This is demonstrated by the steeper dip of unit *uc* (oldest in the basin) in comparison to unit *up* (youngest in the basin), and shows that each of these stratigraphic units was likely involved in a separate (older) event from the unit overlying them, causing these differences in dip angle.

#### Trench 3, southwest wall (refer to Appendix A1 in the electronic supplement)

Trench 3 from Little et al. (2018) was excavated across an active fault strand that lies approximately 1 km to

**Table 2.** Table of samples from Trench 1 and Trench 3 prior to the 2016 earthquake, including radiocarbon ages and sample type (from Table 1 of Little et al. 2018). All these sample ages were used in the updated, preferred age model.

Field Sample Number <sup>^</sup>	Rafter Lab no.	$\Delta 14C^{\#}$ (‰)	Radiocarbon Age <sup>#</sup> (yrs. B.P.)	Calibrated Age* (2 $\sigma$ ) (yrs. B.P.)			Modes		Probability for each 2 $\sigma$ range (%)					unit	Sample type
				1	2	3	4	5	1	2	3	4	5		
<u>Trench 1 (SW)</u>															
Kek-16-T1-1	NZA 61005	-25.0 ± 0.2	176 ± 20	273–204	192–169	153–133	120–57	28–0	39.5	4.2	10.7	27.1	13.5	mp	Charcoal fragments
Kek-16-T1-2	NZA 61009	-24.2 ± 0.2	419 ± 20	498–442	364–331				71.2	23.6				mp	Charcoal fragments
Kek-16-T1-3	NZA 61010	-24.7 ± 0.2	914 ± 20	800–729					94.7					lp	Piece of charcoal
Kek-16-T1-4	NZA 61011	-25.5 ± 0.2	789 ± 20	721–660					95.3					up	2 charcoal fragments
Kek-16-T1-5	NZA 61217	-25.7 ± 0.2	1794 ± 23	1716–1592					95.3					uc	Charcoal fragments
Kek-16-T1-9	NZA 61012	-25.4 ± 0.2	528 ± 20	538–502					95.1					lp	Piece of charcoal
Kek-16-T1-12	NZA 61218	-26.1 ± 0.2	1844 ± 23	1819–1765	1753–1699	1650–1621			27.0	16.4	7.6			uc	Charcoal fragments
<u>Trench 2 (SW)</u>															
Kek-16-T2-1	NZA 61013	-24.8 ± 0.2	1959 ± 21	1921–1822					94.9					gc	Charcoal fragments
Kek-16-T2-4	NZA 61076	-26.3 ± 0.2	1053 ± 22	960–904	862–818				81.7	13.2				gc	Wood fragments
Kek-16-T2-6	NZA 61014	-27.5 ± 0.2	3335 ± 23	3587–3447					94.9					dp	Wood, leaf fragments
<u>Trench 3 (SW)</u>															
Kek-16-T3-1	NZA 61015	-26.0 ± 0.2	1305 ± 20	1270–1169	1145–1093				79.9	15.2				pb	Wood fragments
Kek-16-T3-2	NZA 61006	-24.7 ± 0.2	1044 ± 20	956–902	865–815				70.4	24.6				pa	Piece of charcoal
Kek-16-T3-4	NZA 61007	-27.7 ± 0.2	1802 ± 21	1726–1605					94.9					u-c	Piece of charcoal
<u>Heaver's Creek</u>															
Kek-16-Hc-2	NZA 61008	-26.7 ± 0.2	B/ground	N/A					N/A					N/A	Piece of wood

<sup>^</sup>Final bold number is the one circled and plotted on the trench logs of Figures 6, 7, or 8.

<sup>#</sup>Conventional Radiocarbon Age and  $\Delta 14C$  are reported as defined by Stuiver and Polach (1977).

\*Calibrated with SHCal13 (Hogg et al., 2013). Calibrated ages are reported with respect to AD 1950.

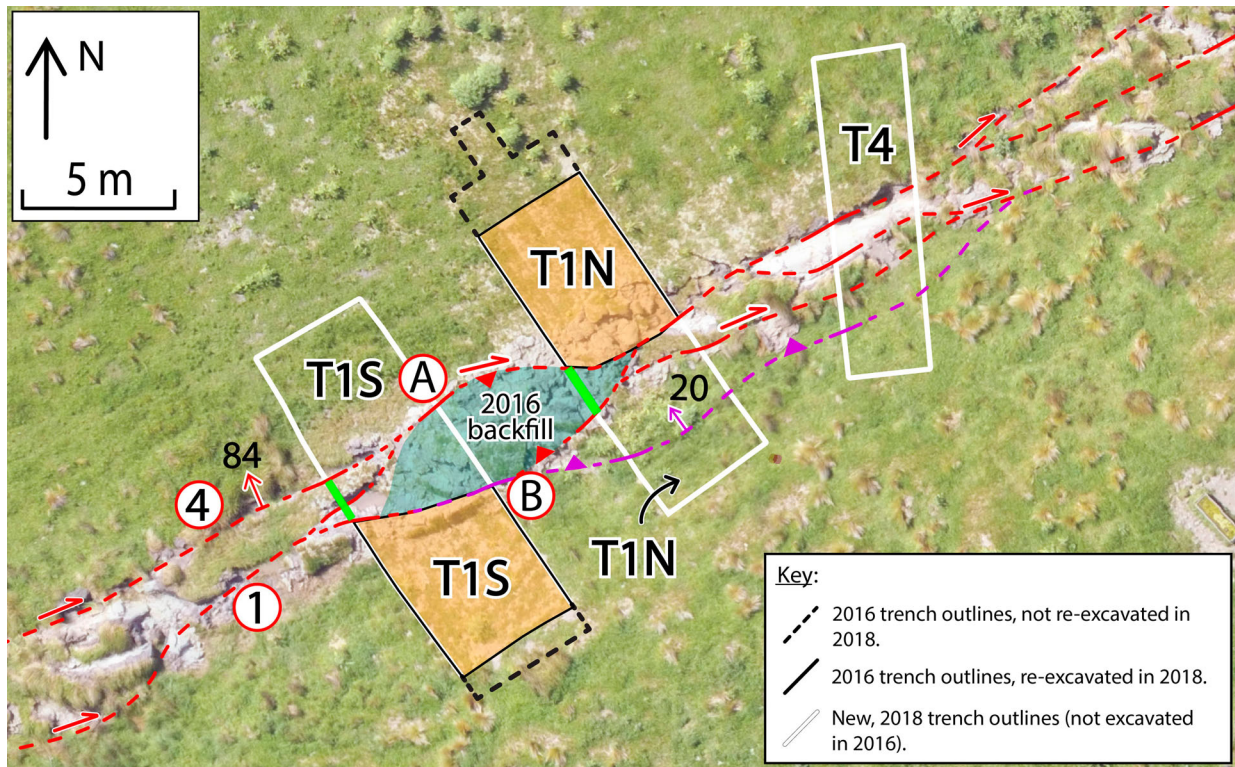


**Figure 4.** Post-2016 site map of trenches T1 and T4 showing 2018 excavations, and fault traces as identified in the trench logs (solid lines) and extrapolated between trenches (dashed lines). Underlying orthophotography was taken by Zekkos (2018) after the earthquake on 28/11/2016. Red faults accommodated strike slip motion in 2016, while purple faults accommodated a combination of strike slip and reverse motion in 2016. Triangles on some faults also show thrust motion. Dip direction is shown by fault perpendicular arrows, with dip angles written adjacent. Numbers 1 and 4 in circles next to faults correspond to numbered faults in the trench logs of Figures 3, 6 and 8. Labels A and B adjacent to faults correlate to faults labelled in Figure 7. Black lines represent 2016 excavation margins, and orange shading represents the displaced halves of the original trench, labelled T1S (southern half) and T1N (northern half). The horizontal extent of the highly deformed central part of the 2016 rupture zone is shown by green bars (which correspond to the bars shown on the trench logs), while the blue shading in this rupture zone shows the location of the earthquake-deformed and up-bulged backfill of the original T1. White lines represent 2018 excavation margins, including the new trench (T4).

the SW of Trench 1 (Figure 2). Only two paleoearthquakes were documented in this trench; the older of these (E4) caused the opening of fissures <1 m deep and <10 cm wide, after which they were infilled and buried by younger sediments. Charcoal samples were taken from the top ~15 cm of the largest fissure's infill for radiocarbon dating (Sample T3-04 (NZA 61007), see Appendix A1 in the Electronic Supplement), and from an overlying clay layer that overlaps the fissure without being cut by it (Sample T3-01 (NZA 61015), see Appendix A1). The ages of these samples were 1726–1605 cal. yrs B.P. and 1270–1093 cal. yrs B.P. respectively. If one interprets the infilling material as younger than the deformational event that opened the fissure, then the age of Sample T3-04 (1726–1605 cal. yrs B.P.) would indicate that there had been a paleoearthquake prior to 1605 cal. B.P. An alternative interpretation is that the infilling material had already existed on or just below the contemporary ground surface at the time of the fissure opening, and that this pre-existing material was redeposited downward into that crack sometime after the earthquake. In this situation, the age of Sample T3-04 (1726–1605 cal. yrs B.P.) would

provide a maximum age for the earthquake that opened the fissure. Because of this ambiguity of interpretation, Little et al. (2018) did not consider further this oldest paleoearthquake or use it in their reconstructed paleoseismic sequence.

### Methods of post-earthquake re-excavation, sampling and age modelling (February 2018, post-earthquake)

#### Excavation

The two displaced fragments (T1N, to the north of the fault; and T1S, to the south) of the pre-earthquake trench, T1, were re-excavated (Figure 4). The trench margins could still be recognised based on the difference in grass density across the trench perimeters—where the trenches had been filled in, the grass was sparse compared to that on the nearby undisturbed ground. Moreover, Real Time Kinematic Ground Positioning Survey points (RTK GPS) along the trench margins were measured both before, and immediately after, the 2016 earthquake (Morris et al. 2021). These surveys affirmed a dextral slip at the site of  $9.0 \pm$

0.3 m, and a strike-orthogonal shortening component (heave) of  $1.3 \pm 0.4$  m (Morris et al. 2021). We exhumed and logged both the NE and SW walls of trench fragment T1S, as well as the SW wall of T1N. Although the original trench, which was benched, was up to  $\sim 4$  m deep in its centre, the re-excavated trench extended only as far down as the bench level, that is to  $\sim 1.75$  m depth, in both of the trench fragments. This limited re-excavation depth was due to water-saturated, unsafe ground conditions at the time of the re-excavation; however, this limitation did not hinder our study because the paleoseismically significant stratigraphy, finely mappable, correlatable and variably deformed (e.g. deformed lenses of organic sediment), is located in the upper metre of the trench.

Trench 3 from Little et al. (2018) was destroyed and unrecognisable after the earthquake due to pervasive ground deformation and was not re-excavated. For the post-earthquake work (see also Morris et al. 2021), we excavated a new,  $\sim 12$  m long trench (T4) located  $\sim 6$  m northeast from trench T1N along the fault trace (Figure 4).

All 2018 trench walls were scraped, cleaned, gridded, flagged, photographed, and logged at a scale of 1:20. Stratigraphic units were described in detail (Appendix A2 in the Electronic Supplement) using, wherever possible, the previously established stratigraphic nomenclature of Little et al. (2018). Several new units were added where necessary; for example, in the new trench (T4), which exposed its own local variant of the stratigraphic sequence.

### Sampling

During the renewed excavations, 28 organic-bearing samples were collected for potential radiocarbon analysis (Table 3). The target material consisted of charcoal fragments, wood, or peat. From these 28, 15 samples were submitted for  $^{14}\text{C}$  analysis. Charcoal samples were preferred as they were deemed most likely to provide the most robust and interpretable approximation of the detrital age of the sediments. Samples were also given priority based on their potential to add precision to the pre-existing (pre-earthquake) stratigraphic and paleoseismic chronology documented by Little et al. (2018); or to extend this chronology further back in time.

In addition to the samples taken during the re-excavation, a further three charcoal samples (PF-01, PF-02, PF-03) were taken from a paleofissure located  $\sim 1$  km to the southwest of the re-excavated trenches (along fault strike, Figure 2). Located along an oblique-normal fault that opened as a deep fissure in 2016 (Figure 5), this fissure preserved clear evidence of a multi-phase opening history. After the 2016 earthquake, the newly reopened

crack was more than a metre wide and 2 metres deep. Its walls exposed a cross-section through a wedge-shaped paleofissure deposit. The three charcoal samples were taken from this paleofissure deposit (Figure 5). The sampled material was not post-2016 infill, but older material that had infilled an older and shallower fissure on the same fault strand during a paleoearthquake (Figure 5). These three samples, as well as the 15 selected samples from new trenches were submitted to the Rafter Radiocarbon Laboratory, Lower Hutt, New Zealand. There, the target organic grains were processed and concentrated by picking, sieving, and chemical pre-treatment. Following processing, the concentrated separates of organic material included charcoal pieces, wood fragments, and undifferentiated plant material, as well as one charcoal rich bulk soil sample (Table 3).

### Age modelling (see appendix 5 in the electronic supplement for OxCal code)

A Bayesian statistical approach was adopted to refine the chronology of the paleoseismic events on the Kekerengu Fault. The original (pre-earthquake) preferred age model from Little et al. (2018) was based on an aggregation of radiocarbon data from Trenches T1 and T3, under the assumption that an event labelled E3 was correlatable between these two trenches. In the present study, one new sample, S1-21 (NZA 67126) from unit *ff* on the NE wall of exhumed T1 (discussed below) was inserted into the pre-existing age sequence to refine the age model based on T1. In addition, three new  $^{14}\text{C}$  ages from for unit *uc* in T1 - samples S1-07 (NZA 67127), S1-20 (NZA 67363), and N1-03 (NZA 67125) - were combined to form a new 'phase' for unit *uc* within that sequence. Samples plotted in phases are 'pooled'—this means that they are not organised in stratigraphic order in the model, rather, they are plotted arbitrarily between two boundaries in a sequence, and therefore provide broader time constraints than sequentially ordered samples. These samples from parts of the *uc* unit were not able to be precisely slotted into the previously established age sequence for that unit, and were therefore aggregated into a generic 'phase' for this unit.

Additionally, a new sequence ('Sequence Trench 4') was created for samples T4-01 (NZA 67358) and T4-09 (NZA 67361) that were dated in trench T4. Because T4 was entirely new, and physically disconnected from the offset fragments of T1, samples collected from it could not be assigned into the paleoseismic sequence for T1; however, the peat unit (*pt*) could be correlated between them on the basis of its physical similarity to the peat sequence in T1 (units *lp*, *mp* and *up*), and the similarity in age between sample T4-09 (904-735 cal.

**Table 3.** Table of samples that were collected in 2018 after the 2016 Kaikōura earthquake, from T1, T4, and the paleofissure site ~100 m southwest of these trenches (see Figure 2). Table includes samples number, radiocarbon age, calibrated age ( $2\sigma$ ), and sample content (i.e. charcoal, wood). Samples highlighted in green were used in the preferred age model (along with samples shown in Table 2), samples highlighted in blue are pooled samples (see Appendix A4 in the Electronic Supplement), red and white highlighted samples were not included in the preferred age model, and orange highlighted samples were used in the alternative age model only (from the paleofissure site).

Field Sample Number	Rafter Lab no.	$\Delta^{14}\text{C}^{\#}$ (‰)	Radiocarbon Age <sup>#</sup> (yrs. B.P.)	Calibrated Age* ( $2\sigma$ ) (yrs. B.P.)			Modes	Probability for each $2\sigma$ range (%)				unit	Sample type
				1	2	3		1	2	3	4		
<u>Trench 1 (SW)</u>													
Kek-18-S1-03	NZA 67128	-25.0 ± 0.2	618 ± 24	632–596	567–533			48.6	51.4			fp	single charcoal fragment
Kek-18-S1-06	NZA 67364	-27.4 ± 0.2	Modern									fp	Plant material
Kek-18-S1-07	NZA 67127	-24.7 ± 0.2	2178 ± 23	2300–2244	2178–2168	2161–2042	2030–2018	15.9	1.5	81	1.7	uc	Wood
Kek-18-N1-01	NZA 67365	-26.7 ± 0.2	Modern									bp	Plant material
Kek-18-N1-02	NZA 67129	-25.7 ± 0.2	2005 ± 23	1997–1945	1943–1870	1850–1839		30.1	66.9	3		ml	Charcoal fragments
Kek-18-N1-03	NZA 67125	-25.4 ± 0.2	1808 ± 23	1734–1605	1599–1594			99.1	0.9			uc	Charcoal fragments
<u>Trench 1 (NE)</u>													
Kek-18-S1-20	NZA 67363	-24.3 ± 0.2	1664 ± 23	1570–1429				100				uc	Wood
Kek-18-S1-21	NZA 67126		949 ± 22	905–851	844–825	824–745		38.6	5.5	55.9		ff	Charcoal fragments
Kek-18-S1-22	NZA 67362	-24.4 ± 0.2	454 ± 23	511–451	351–340			95.9	4.1			ff	Charcoal fragments
Kek-18-S1-23	NZA 67300	-27.2 ± 0.2	1529 ± 20	1408–1316				100				uc	soil
<u>Trench 4 (SW)</u>													
Kek-18-T4-01	NZA 67358	-24.7 ± 0.2	1857 ± 24	1824–1702				100				ffb	Charcoal fragments
Kek-18-T4-06	NZA 67301	-27.8 ± 0.2	Modern									pt	Plant material
Kek-18-T4-07	NZA 67359	-24.2 ± 0.2	1784 ± 24	1710–1587				100				ml	Charcoal fragments
Kek-18-T4-08	NZA 67360	-24.9 ± 0.2	1799 ± 24	1723–1593				100				ml	Charcoal fragments
Kek-18-T4-09	NZA 67361	-26.1 ± 0.2	937 ± 23	904–861	841–829	819–735		24.3	1.9	73.8		pt	Wood
<u>Benmore Paleofissure Site</u>													
Kek18-PF-01	NZA 65131	-25.1 ± 0.2	2220 ± 20	2300–2240	2180–2148			43.3	24.9				Charcoal fragments
Kek18-PF-02	NZA 65132	-25.0 ± 0.2	2200 ± 20	2296–2260	2174–2171	2158–2141	2132–2096	24.3	1.5	14.5	27.8		Charcoal fragments
Kek18-PF-03	NZA 65133	-24.9 ± 0.2	2196 ± 20	2295–2264	2157–2140	2133–2094		20	14.8	33.2			Charcoal fragments

\*Calibrated with SHCal13 (Hogg et al. 2013). Calibrated ages are reported with respect to AD 1950.

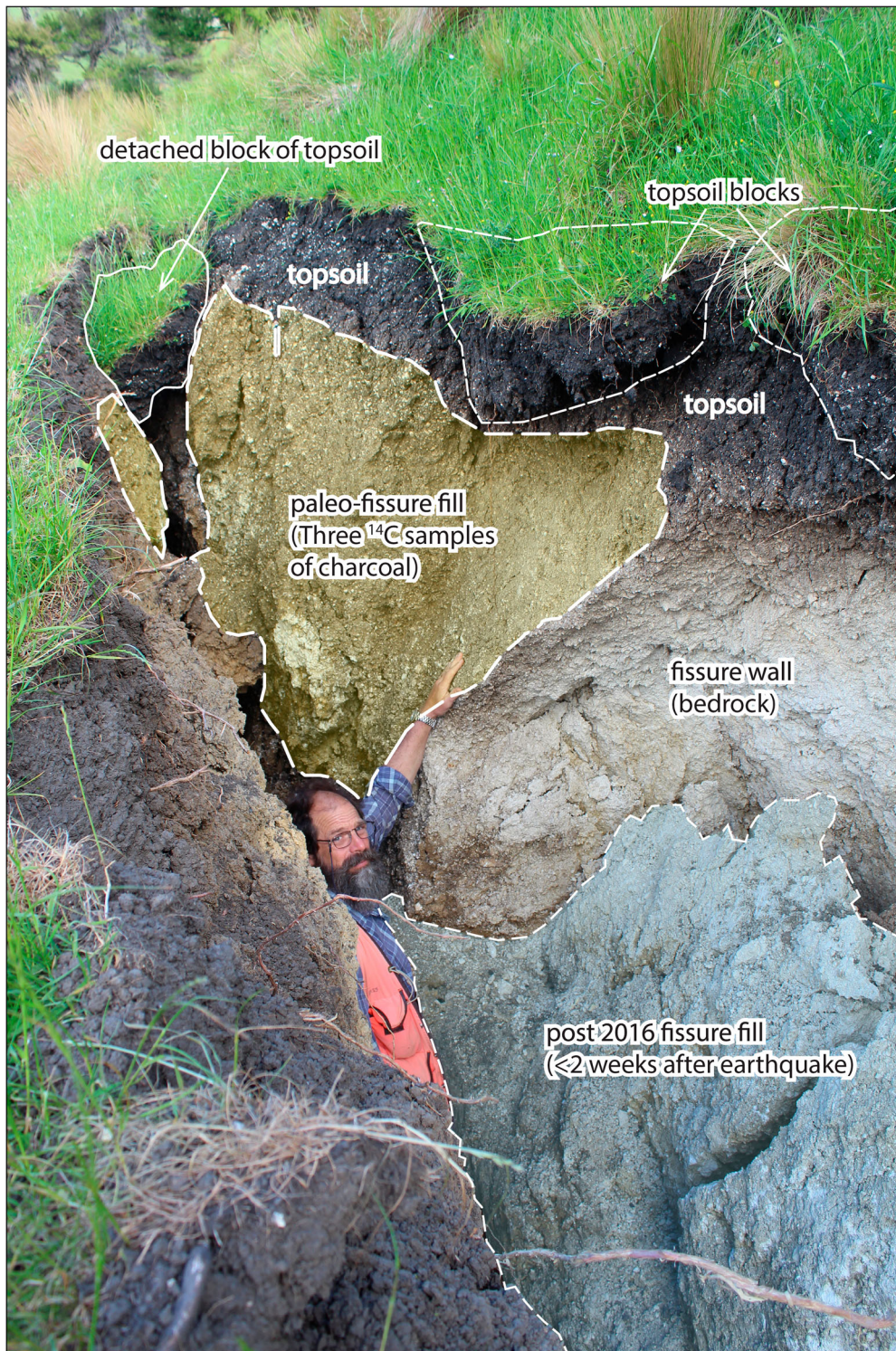


**Figure 5.** Paleofissure that re-opened on the Kekerengu Fault during the 2016 Kaikōura earthquake, located ~100 m southwest of Trench T1 along fault strike, and ~25 m southwest of Trench T3 along fault strike (see Figure 2). Paleofissure infill is shaded yellow, while the deepened cavity that opened in 2016 is what the geologist is occupying. Three radiocarbon samples were taken from this paleofissure fill (shaded yellow), which were used to constrain the timing of paleoearthquake E5 (see text). Photograph was taken in November 2016 approximately 2 weeks after the earthquake, and the paleofissure has already been rapidly infilled by a) slabs of fissure wall (shaded blue) which likely collapsed during the earthquake, and b) blocks of topsoil on the ground surface proximal to the fissure (such as those that are labelled on the photograph). This paleofissure was surveyed again ~2 years after the earthquake and was almost completely infilled by material derived from the collapse of its walls, and toppled topsoil blocks. Photography by Kate Clark.

ys B.P) from unit *pt* and sample S1-21 from unit *ff* in T1 (905-745 cal. yrs B.P.). Combining all the pre- and post-earthquake age data together based on an argued set of correlations (see results—age modelling and

chronology), resulted in a newly expanded age model produced for the paleoearthquake events on this part of the Kekerengu Fault, using the programme OxCal 4.2.3 and following methods outlined in Bronk

Ramsey (2008) and Lienkaemper and Bronk Ramsey (2009). This new model incorporates all the radiocarbon data from the pre-2016 earthquake trenches T1 and T3 as presented in Little et al. (2018), plus new data from the post-earthquake trenches; that is, the re-excavated walls of the southern trench fragment T1S (both the SW and NE walls) and the northern trench fragment T1N (SW wall only), as well as the entirely new trench, T4 (SW wall). The expanded data set results in a new preferred age model that is based on 16 radiocarbon samples (as opposed to the 10 samples in the original age model).

## Trenching results

### Post-earthquake stratigraphy and cross-cutting relationships (2018)

The re-excavated, extended fragments of the original displaced trench were re-logged to document changes in stratigraphy, cross-cutting relationships, and geological structures. Here we focus only on new information that refines the paleoseismic chronology of the Kekerengu Fault. Table 1 compiles evidence for events E1, E2 and E3 both before and after the earthquake, detailing which of these paleoevents are still recognisable in the stratigraphic record of each of the T1 trench walls following the deformation in 2016. For an analysis of the coseismic

deformation in 2016 based on the changes in stratigraphic relationships, the reader is referred to Morris et al. (2021).

### T1S, SW wall (refer to Figure 6)

To the northwest of fault 4, material has been displaced into the plane of view of the trench wall from the southwest. The presence of almost identical stratigraphic units and sequence on this faulted trench wall to those originally logged in 2016 suggests that the 'faulted-in' stratigraphy was laterally continuous along strike to the SW, and thus did not change much in this plane of view, despite metres of co-seismic, out-of-plane motion. To the southeast of fault 1, the trench wall consists of the same material as was exposed in the original trench, but is now much tilted and deformed. On this part of the wall, we recovered buried nails and string (artefacts left behind from the original trenching investigation in January 2016). Between faults 1 and 4 is a strongly deformed part of the rupture zone that includes the NW-dipping limb of the central syncline. Relative to the pre-earthquake log (Figure 3), the stratigraphy in the post-earthquake trench between faults 1 and 4 (Figure 6) is slightly altered; for example, with steepened bedding dips, because of pervasive strike-slip shearing and/or rotation of sediment blocks into the plane of view during the earthquake (Morris et al. 2021). Evidence for event E1 was destroyed on this trench wall in

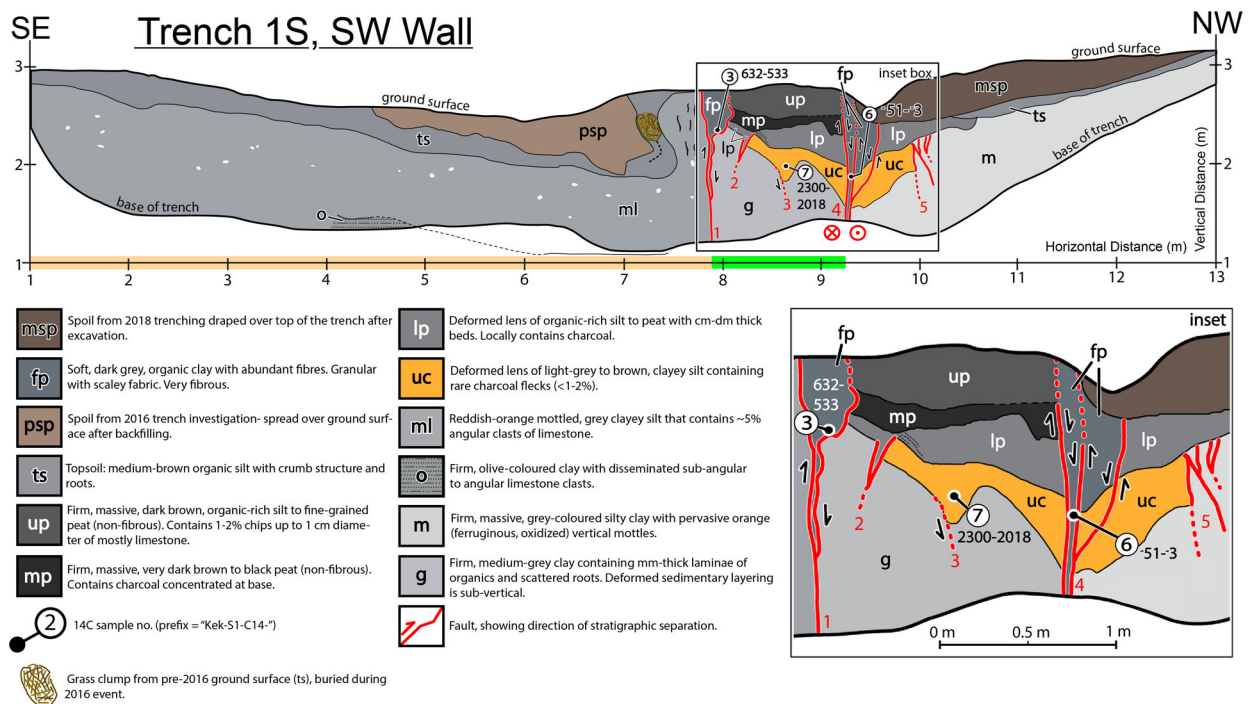


**Figure 6.** Log of the re-excavated (2018, post-earthquake) southwest (SW) wall of Trench T1, fragment 1S, showing numbered faults and basic stratigraphy.  $^{14}\text{C}$  age ranges are quoted in cal. B.P. at 95% confidence (negative ages are given where samples were younger than 1950 AD). For more information on the  $^{14}\text{C}$  samples, see Table 3. Orange highlight along the scale bar below the trench log identifies material that is exactly the same as that logged in the pre-earthquake trench (but contractionally deformed). Lime green bar shows the extent of the central, highly deformed part of the 2016 rupture zone, also shown enlarged in the inset (labelled). No vertical exaggeration.

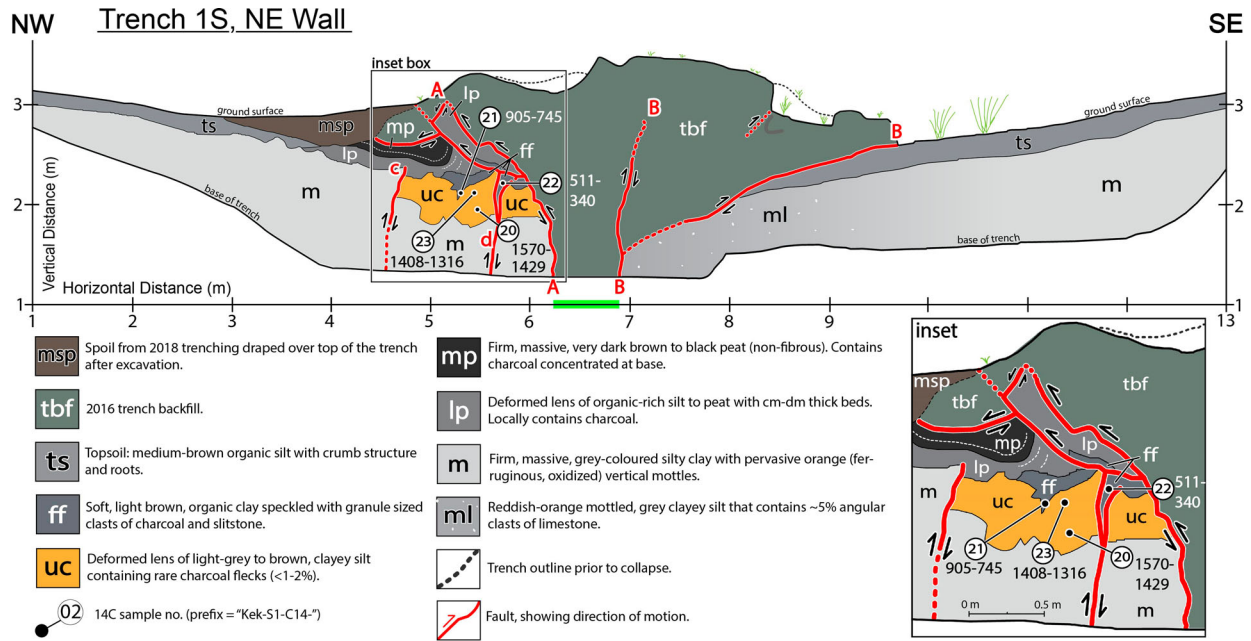


**Figure 7.** Post-earthquake log of northeast (NE) wall of Trench T1S. Faults bounding the central part of the 2016 rupture zone (extent shown by lime green bar underneath the trench log) are labelled A and B (see also Figure 4); fault 'c' is labelled to the NW of this rupture zone. Inset (labelled) shows enlarged version of the displaced, original stratigraphic sequence, just to the NW of the central 2016 rupture zone.  $^{14}\text{C}$  age ranges are quoted in cal. B.P. at 95% confidence. For more information on the  $^{14}\text{C}$  samples, see Table 3. No vertical exaggeration.

2016, but despite this deformational overprinting, evidence for events E2 and E3 are still observed on this wall (see Table 1).

Three radiocarbon samples were taken from this trench wall, the significance of which are discussed in the section 'Revised Chronology and Age Modelling (2018)'. These samples were each submitted for radiocarbon dating: Samples S1-03 (NZA 67128, 632–533 cal. yrs B.P.) and S1-06 (NZA 67364, modern age) were taken from within structures that formed in the 2016 earthquake to see if they returned modern ages and thereby 'test' paleoseismic methods, while Sample S1-07 (NZA 67127, 2300–2018 cal. yrs B.P.) was taken from unit *uc* to potentially further constrain the maximum age of E3 established by Little et al. 2018.

### T1S, NE wall (refer to Figure 7)

During the 2016 earthquake, material to the NW of a major strike-slip fault strand labelled 'A' (Figure 4) was translated into the plane of this trench wall from an original location several metres to the SW. This 'shunted in' material contains a sequence of units (Figure 7) similar to that exposed on the opposite (SW) wall of the trench (both pre- and post-earthquake versions, Figures 3 and 6). The NE wall of this trench exposed one new unit (unit *ff*) that was unique to that wall. This lens of organic clay lies stratigraphically between the previously defined units *uc* and *lp*. Charcoal fragments from unit *ff*, sample S1-21 (NZA 67126) were dated at 905–745 cal. yrs B.P., which overlaps with an age that Little et al. (2018) obtained for the *lp* unit (sample T1-3 (NZA 61010), 800–502 cal.

yrs B.P.). We interpret unit *ff* to be a lighter coloured part of the lower *lp* unit that had been deposited several metres to the southwest of the original T1 excavation, and that was translated into the plane of view of this trench wall during the 2016 earthquake.

On this trench wall, the central rupture zone between faults A and B bounds an up-bulged mass of deformed backfill (unit *tbf*) from the 2016 excavations. The fault furthest to the NW from this mass, (which we did not confidently correlate to any faults on the opposite trench wall) offsets the *uc* unit and the base of *lp* but does not cut through the overlying *mp* unit, providing further evidence (in a new location) for earthquake E2 of Little et al. (2018) (see Table 1). If any evidence for events E1 and E3 were present in the material of this trench wall prior to the 2016 earthquake, that evidence was destroyed in 2016 when the backfill (*tbf*) was rotated, up-bulged and internally sheared between faults A and B (Morris et al. 2021).

In addition to Sample S1-21 (previously mentioned), three other radiocarbon samples taken from this trench wall were submitted for radiocarbon dating. The paleoseismic significance of the ages of these samples is further discussed in the section 'Revised Chronology and Age Modelling (2018)'. Samples S1-20 (NZA 67363, 1570–1429 cal. yrs B.P.) and S1-23 (NZA 67300, 1408–1316 cal. yrs B.P.) (Table 3) were taken from unit *uc*, to potentially further constrain the maximum age of E3 established by Little et al. 2018, while Sample S1-22 (NZA 67362, 511–340 cal. yrs B.P.) was taken from the new unit *ff*.

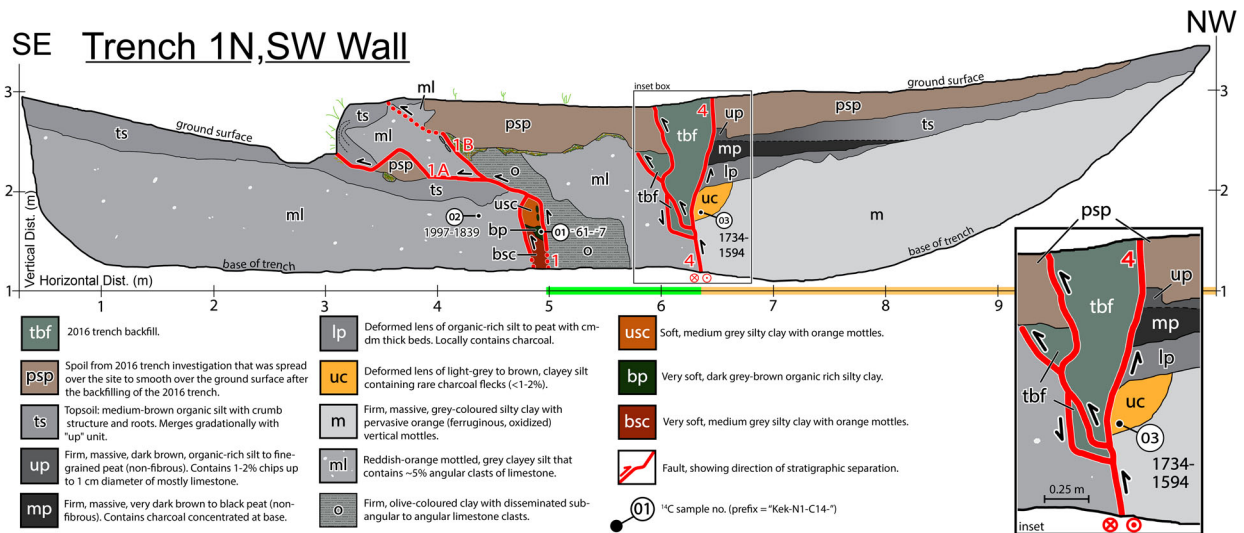


**Figure 8.** Log of the SW wall of Trench T1N, showing numbered faults (1 and 4, correlated to original 2016 trench) and basic stratigraphy. Orange highlight along the scale bar below the trench log identifies the horizontal extent of material that was logged in the pre-earthquake (2016) trench. Lime green bar underneath the central part of the trench log represents the central part of the 2016 rupture zone.  $^{14}\text{C}$  age ranges are quoted in cal. B.P. at 95% confidence (negative ages are given where samples were younger than 1950 AD). For more information on the  $^{14}\text{C}$  samples, see Table 3. Inset (labelled) shows the enlarged version of the northeastern tail end of the trench backfill from the 2016 excavation (unit *tbf*), displaced into plane from the SW. Green pods sketched underneath the unit *psp* represent grass clumps from the pre-earthquake trench excavation. No vertical exaggeration.

### T1N, SW wall (refer to Figure 8)

Material to the NW of fault 4 on this wall of the post-earthquake trench T1N (Figure 8) is equivalent to that logged in the pre-earthquake trench, T1 (Figure 3). This material is a fault-truncated segment of the south-dipping limb of the central syncline. Everything to the SE of fault 4 is ‘allochthonous’ with respect to the original wall of trench T1 (Figure 3), as it has been translated into the plane of view from an original depositional site farther to the NE. The upwardly bifurcating trio of faults labelled ‘fault 4’ in Figure 8 was the major locus of dextral displacement during the 2016 earthquake, and this fault zone encloses a wedge of T1 backfill (unit *tbf*) that was pervasively sheared during the 2016 earthquake. Between faults 1 and 4, units *o* and *ml* have been tilted NW and uplifted along fault 1. The overturned topsoil (unit *ts*) on this upthrust wedge has translated to the SE and overridden the same material in the footwall, thus partially burying the pre-2016 ground surface. Evidence for E2 and E3 are still preserved on this wall after the 2016 earthquake (see Table 1).

Three radiocarbon samples taken from this trench wall were submitted for radiocarbon dating; the significance of their ages is discussed in ‘Revised Chronology and Age Modelling (2018)’. Sample N1-01 (NZA 67365, modern age) was taken from unit *bp* as this new unit (as well as units *usc* and *bsc*) was suspected to be older than any of the stratigraphy described by Little et al. 2018, thrust up above unit *ml* by fault 1 in the 2016 earthquake. Based on the modern radiocarbon age of Sample N1-01, this trio of units was later interpreted as the in-fill of a fissure that was both formed

and overridden in the 2016 rupture (see ‘Implications for future paleoseismic studies’ in the discussion section of this paper). Sample N1-02 (NZA 67129, 1997–1839 cal. yrs B.P.) was taken from unit *ml* to provide more age information on the original stratigraphic sequence established by Little et al. 2018, as this unit was not dated in this previous study. Sample N1-03 (NZA 67125, 1734–1594 cal. yrs B.P.) was taken from the unit *uc*, again to potentially constrain further the maximum age of E3 described in Little et al. 2018.

### Trench 4, SW wall (refer to Figure 9, also Appendix A3 in the Electronic supplement):

This trench was dug into previously unexcavated material on both sides of the rupture zone at a location about 5 m to the northeast of T1N (see Figure 3). Most stratigraphic units exposed in T4 cannot be correlated with those in T1 (or that trench’s fault-displaced fragments T1N and T1S).

Deeply penetrating, elongate, fault-bounded wedges of organic-rich material are exposed in the central rupture zone of this trench (Figure 9 inset). They resemble fissures that Little et al. (2018) observed prior to the 2016 earthquake in their T3 trench (Appendix A1, Electronic Supplement), and we similarly interpret them as fissures that had been infilled during one or more paleoearthquakes prior to 2016. The inferred fissure furthest to the NW along the trench wall (label g, Figure 9) contains blocky peat (unit *ffb*), which is overlain by a peat layer (unit *pt*). The same sequence is observed in another larger (>1 m long) fissure on the southeast side of the central rupture zone (label e, Figure 9). We interpret that the

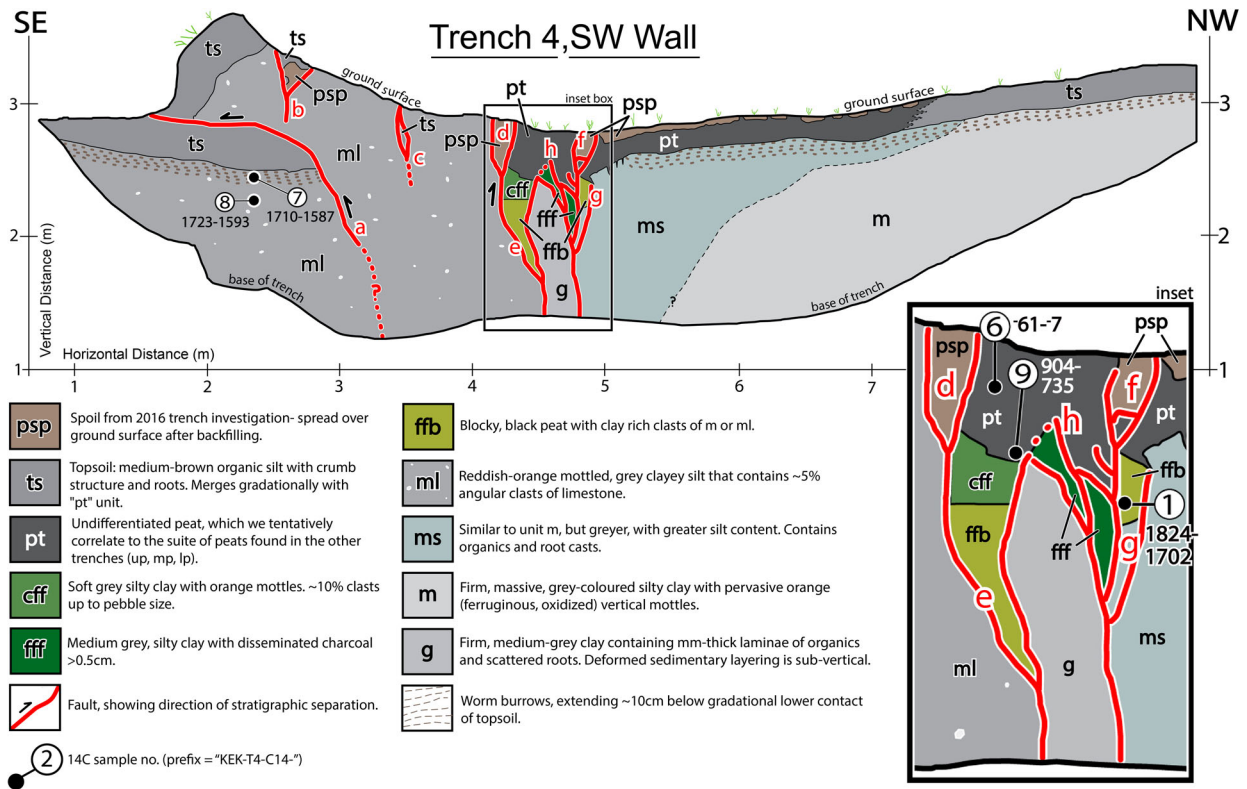


**Figure 9.** Log of SW wall of Trench T4, showing faults and basic stratigraphy. Faults could not be correlated to those in T1S and T1N, and so are labelled with letters for ease of reference in the text. Inset shows enlarged version of the main faults in the trench, and the  $^{14}\text{C}$  age ranges, quoted in cal. B.P. at 95% confidence (negative ages are given where samples were younger than 1950 AD). For more information on the  $^{14}\text{C}$  samples, see Table 3. No vertical exaggeration.

stratified infill material may have been derived from up to two paleoearthquakes: first, unit *ffb* filled in the lower part of the fissure soon after a paleoearthquake. This layer was subsequently buried by a silty clay, unit *cff*, perhaps in the subsequent post-seismic interval. Then, a possible second paleoearthquake reopened and deepened the fissure, after which the organic-rich unit *pt* was deposited into and buried its upper part (we note that this sequence of deposits may be the result of a single earthquake). The same sequence occurs in the smaller fissure labelled *g*.

To date these inferred paleoearthquakes, three charcoal infill samples were submitted for radiocarbon dating: T4-01 from *ffb* (NZA 67358, 1824–1702 cal. yrs B.P.), and T4-06 (NZA 67301, modern age) and T4-09 (NZA 67361, 904–735 cal. yrs B.P.) from *pt*. In addition to these, Samples T4-07 (NZA 67359, 1710–1587 cal. yrs B.P.) and T4-08 (NZA 67360, 1723–1593 cal. yrs B.P.) were taken from the unit *ml*, to provide further age information on the original stratigraphic sequence established by Little et al. (2018). The paleoseismic significance of all five of these samples is discussed in the following section, ‘Revised Chronology and Age Modelling (2018)’.

Evidence of the 2016 earthquake is also clear on this trench wall. A large fault is observed on the southeast side of the trench (label a, Figure 9) which up-thrusts the modern topsoil (unit *ts*) to form a moletrack at the surface (see Appendix A3 in the Electronic

Supplement for orthomosaic). Additionally, the spoil from the 2016 excavations (unit *psp*) and the modern, previously undeformed topsoil (*ts*) can be seen juxtaposed by faults against older stratigraphic units (units *pt* and *ml*) in several places (see labels b, c, d, and f on Figure 9).

### Revised chronology and age modelling (2018)

#### Samples included in the new, preferred age model (2018 excavations)

Of the 18 samples submitted for radiocarbon analysis in this study, only six were incorporated into the revised (preferred)  $^{14}\text{C}$  age model (Table 3). The dates that were selected were those that could be confidently slotted into the stratigraphic sequence of Little et al. (2018), and thus strengthen (and make more precise) the age model and its derived earthquake chronology. Sample S1-21 (NZA 67126) from unit *ff* in T1S was inserted into the pre-existing stratigraphic sequence. This sample, by yielding another age estimate for unit *lp* (in particular near its base) provides a slightly (~30 yrs) older minimum age for E3 (905–745 cal. yrs B.P.) than previously established by Little et al. (2018).

For some of the new  $^{14}\text{C}$  samples, we could not confidently assign a precise internal stratigraphic ordering relative to the samples in the original age model of Little et al. (2018)—particularly when the

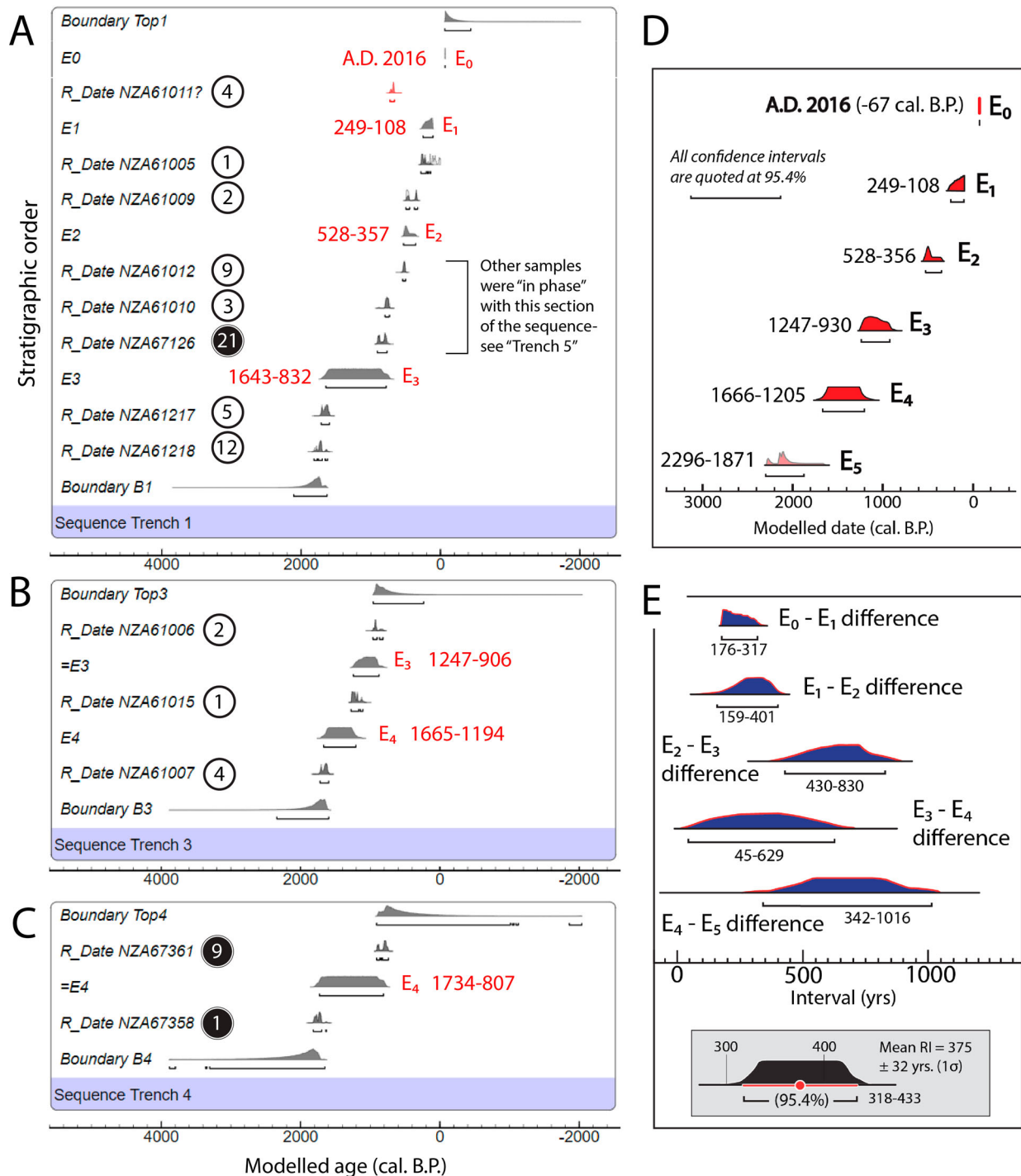


**Figure 10.** Age modelling results: **A**, **B**, and **C**, show the sequences for trenches T1 (also T1N and T1S), T3 and T4 respectively, showing samples in stratigraphic order, with youngest at the top (modified from Little et al. 2018). Events are labelled in each trench sequence with age ranges based on samples from individual trenches only, rather than a correlation between trenches. White numbered circles are samples collected in 2016, whereas black numbered circles are samples collected in 2018; **D**, Modelled probability density functions for each paleo-event, including E<sub>5</sub> (not necessarily immediately preceding E<sub>4</sub>); **E**, Modelled probability density functions for the intervals between paleo-events, showing the re-calculated mean recurrence interval (RI) for the fault, and the probability density function for the RI.

relative positioning of a dated sample within the thickness of previously recognised stratigraphic unit was unclear with respect to pre-earthquake <sup>14</sup>C samples that were collected in January 2016. These spatial-stratigraphic ambiguities between samples arose because of changes in shape and thickness of units as a result of deformation and out-of-plane motion during the 2016 earthquake (although the stratigraphic unit

identity of the sample was clear). Accordingly, three samples from the *uc* unit were entered into the new age model as a 'phase' for that unit rather than as part of an ordered sequence of samples (see Appendix A4 and A5 in the Electronic Supplement). This 'phase' combines samples S1-07, S1-20, and N1-03 (NZA 67127, NZA 67363 and NZA 67125, respectively). They strengthen our dating of unit *uc*, which must

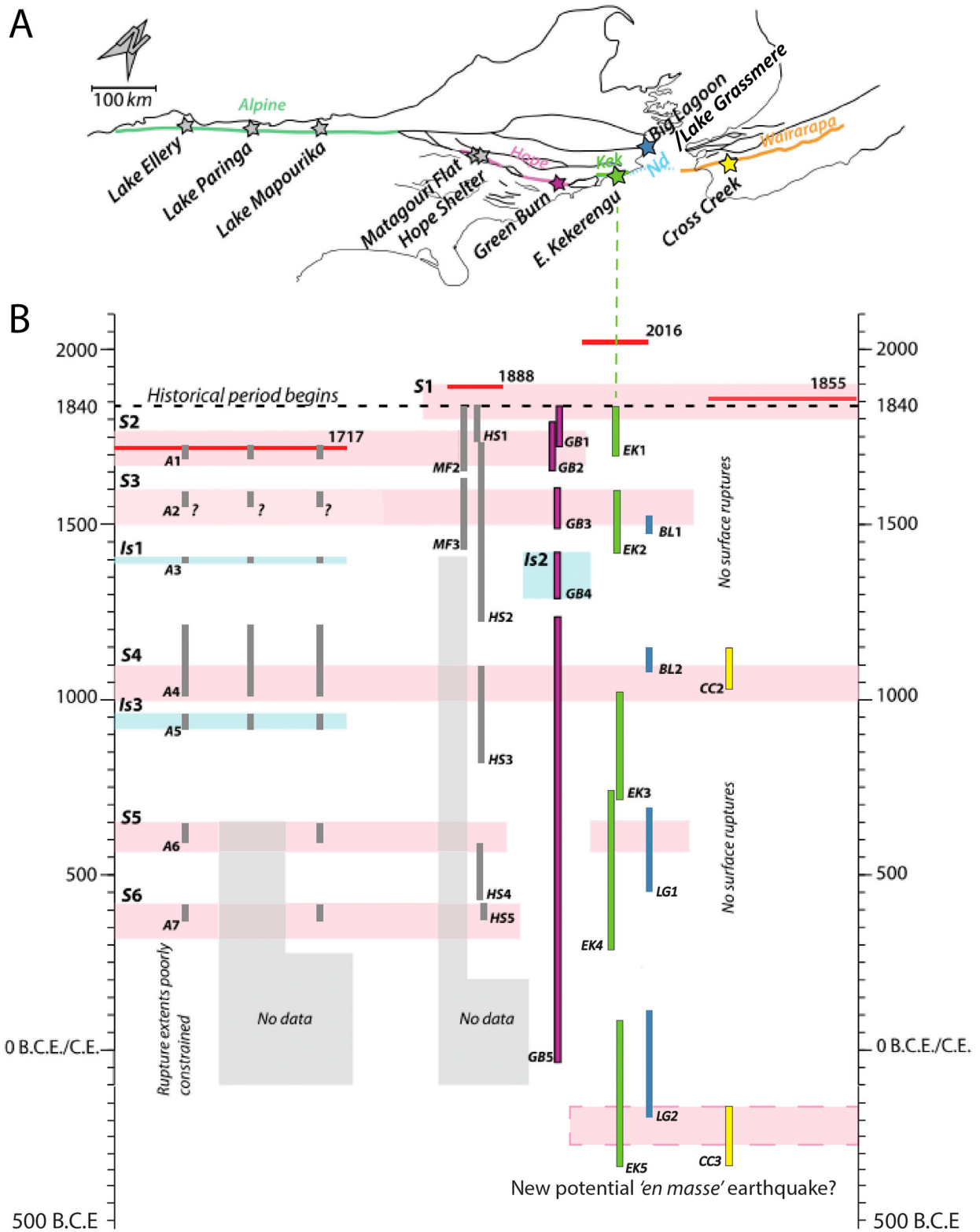


**Figure 11.** Updated compilation of the paleoseismological data from the Alpine (Wells et al. 1999; Howarth et al. 2018), Hope (Langridge et al. 2003; Langridge et al. 2013; Khajavi et al. 2016; Hatem et al. 2019), Kekerengu-Needles (this study, Pizer et al. 2021) and Wairarapa (Little et al. 2009) Faults, adapted from Hatem et al. (2019); **A**, Map with labelled active faults and paleoseismic sites; **B**, Space-time diagram: thin, vertical bars show the possible temporal range of dated earthquakes (2σ age range), labels correspond to sites plotted in **A** (i.e. EK4 corresponds to the Eastern Kekerengu Fault, paleoearthquake E4). Pink horizontal bands represent 100-year-long time intervals of possible overlapping ruptures at different sites (after Hatem et al. 2019). These highlight potential cases of 'en masse strain release', or many earthquakes happening in a short time frame. Blue horizontal bars identify apparent single-fault earthquake ruptures.

predate E3 (Figures 6, 7, and 8). In our new preferred age model, these pooled ages for *uc* are assigned to a 'virtual trench' (Trench 5) in the programme OxCal

(see 'Methods'). This allows these ages to provide further constraints regarding the maximum age for E3, but weights them less heavily than the

stratigraphically well-ordered samples in *uc* that were mapped prior to the earthquake by Little et al. (2018).

According to our fissure-infill interpretation for the fault-bounded wedges *e* and *g* in T4 (Figure 9), Samples T4-1 (NZA 67358) and T4-9 (NZA 67361) must pre- and post-date, respectively, a paleoearthquake, or possibly two. The age of sample T4-1 from *ffb* is 1824–1702 cal. yrs B.P., whereas T4-9 from unit *pt* is 904–735 cal. yrs B.P. Together they bracket a paleoearthquake that occurred several hundred years prior to E3 of Little et al. (2018). Following the infilling of this fissure, the *pt* unit was cut by a fault (labelled *h*) during a younger earthquake. We note that in T4 the age of Sample T4-9 in the *pt* unit (904–735 cal. yrs B.P.) is indistinguishable from that of Sample S1-21 in unit *ff* in T1S (905–745 cal. yrs B.P., Figure 7). This suggests that they are equivalent peaty deposits, and we correlate both with unit *lp* in the original T1. In our new age model, all these ages are assigned to the *lp* unit with the new ages for unit *ff* (T1S) and *pt* (T4) being assigned to an internally unordered (‘phase’) version of *lp*. In the model, all dates for the unit *lp* must predate earthquake E3.

Finally, the age of Sample T4-1 (1824–1702 cal. yrs B.P.) in the fissure-infilling unit *ffb* is indistinguishable from that of another fissure infill deposit that Little et al. (2018) dated in their in Trench 3 (Sample T3-4, 1726–1605 cal. yrs B.P., see Appendix A1 in the Electronic Supplement). As these samples of organic-rich silt both infill deep fissures of similar morphology, and while they are located in different trenches, we attribute them to a common paleoearthquake older than E3. Following Little et al. (2018), we call this earthquake E4.

#### **Samples omitted from the new, preferred age model (2018 excavations)**

The other nine samples that were submitted for radiocarbon dating were not incorporated into our new age model. Three  $^{14}\text{C}$  samples were collected from the *ml* unit (Samples N1-02, T4-07, and T4-08, see Table 3), part of the thick layer of silt beneath the central peaty syncline in trench T1N and T4. The results span an age range of 1997–1593 cal. yrs B.P., and thus occur in the correct stratigraphic order with the other units in the sequence. They reinforce the dating of our stratigraphic sequence, but they do not help to bracket or refine the age of any of the currently identified surface-rupturing earthquakes, and so they were omitted from the new preferred age model.

In the southern fragment of T1, Sample S1-22 from unit *ff* yielded an age of 511–340 cal. yrs B.P. (Figure 7). This result was omitted from the new age model because the unit *ff* is fault-bounded here and has an unknown stratigraphic relationship to any of the other samples. Also in that trench, Sample S1-23 (1408–1316 cal. yrs B.P., Figure 7) was a bulk, charcoal

rich soil sample taken from the unit *uc* that predates paleoearthquake E3. At 1408–1316 cal. yrs B.P., the age for this sample was significantly younger than the other 4 internally accordant ages for that unit (see Figure 3, Figures 6–8, and Tables 1 and 2). For this reason, we inferred that the charcoal flecks in this sample may have been incorporated into the soil after deposition, and we have not used it in the new model.

To ‘test’ paleoseismic methodology, we submitted several samples of faulted modern topsoil, that in theory ‘should’ closely predate the age of the 2016 earthquake. In T1S, these included samples S1-03 (NZA 67128) and S1-06 (NZA 67364), both from organic-rich soils that were cut in the near-surface by splays of the 2016 rupture (Figure 6). Sample S1-03 yielded age of 632–533 cal. yrs B.P., whereas Sample S1-06, as expected, yielded a modern one. Based on its ‘unexpectedly’ old age, the former sample is interpreted to be part of a laterally displaced fault sliver of the *lp* unit. In trench T1N, Sample N1-01 (NZA 67365) from unit *bp* occurs as a structurally buried remnant of modern topsoil (that was overthrust within a mole-track in 2016) and yielded a modern age (Figure 8). In trench T4, Sample T4-6 (NZA 67301), which is from faulted peaty material within 15 cm of the 2018 ground surface, also yielded a modern age (Figure 9). None of these ages were included in the new preferred age model because we already know the age of the youngest surface-rupturing event exactly (14 November, A.D. 2016), so these ages add no useful chronological information.

#### **Newly revised, preferred age model**

Our new preferred age model for the timing of paleoseismic events on the Kekerengu Fault is based on 16 samples in total: 10 pre-earthquake samples from Little et al. (2018), and 6 new post-earthquake samples, as outlined above. Based on our recognition and formulation of E4, this new model now includes four paleoearthquakes in addition to the 2016 event (Figure 10), one more than was recognised by the Little et al. (2018) study. The modelled earthquake ages (in cal. yrs B.P.) are: 249–108 (E1), 528–356 (E2), 1247–930 (E3), and 1666–1205 (E4) cal. yrs B.P. (at 95% confidence, Figure 10D). Apart from the newly added older event, E4, these ages do not differ much from those determined in the previous age model by Little et al. (2018). The main change is that the maximum age bracketing for E3 has now been reduced (i.e. made more precise) by ~30 yrs.

Based on data from their T3 trench, Little et al. (2018) speculated about the age of E4 but did not model this event due to the ambiguity in interpreting fissure infill samples as maximum or minimum ages. Following the 2016 earthquake, however, field

observations showed that most of the fissures that opened during 2016: 1) were largely infilled in <2 years; and 2) this infilling material consisted of topsoil and/or colluvium that had existed on (or just below) the ground surface prior to earthquake. This was true for the remarkably deep fissure depicted in [Figure 5](#), into which we observed that large masses of the pre 2016 topsoil toppled downward to partially fill it. If dated, the age of such downwardly redeposited material would thus be older than (or indistinguishable from) A.D. 2016, and would provide a maximum limiting age for the earthquake. We can now confidently infer that the  $^{14}\text{C}$  ages of fissure-infilling material (including paleofissure infill) along this stretch of fault (and presumably also along faults with similar depositional settings – i.e. where fissure walls and adjacent slopes are composed of relatively easily erodible material and where there are sufficient mechanisms (such as rainfall) to move that material) do not provide minimum age constraints for fissure-opening earthquakes, but maximum ones. This is because the infill consists chiefly of recycled material that has toppled downward into the crack, rather than juvenile organic material that was formed and deposited after the earthquake. Once a fissure is filled in, any younger layers draped over the fissure will potentially provide minimum age constraints for the fissure-opening earthquake. Thus, we are now able to bracket the age of E4, using a combination of fissure infill samples from Trench 3 (old, re-interpreted - T3-4 as a maximum age, T3-1 as a minimum age, see Appendix A1 in the Electronic Supplement) and T4 (new samples, T4-01 as a maximum age, T4-09 as a minimum age; refer to [Figure 9](#)).

This new preferred age model includes these four paleoearthquakes as well as the 2016 earthquake and calculates a revised mean recurrence interval (RI) for the Kekerengu Fault of  $375 \pm 32$  yrs ( $1\sigma$ ) ([Figure 10E](#)), which is almost identical to the RI presented in [Little et al. \(2018\)](#). This concordance is reassuring, because it reflects the internal stratigraphic consistency in the 16 total  $^{14}\text{C}$  samples (six of them new) that have been brought together to make our updated age model.

### **Alternative, expanded age model**

The three charcoal samples that were taken from the large paleofissure ~1 km southwest of T1 along fault strike ([Figures 2](#) and [5](#)) were remarkably similar in age to one another, at 2300–2148, 2296–2096, and 2295–2094 cal. yrs B.P. respectively ([Table 3](#)). As argued in the previous section, these samples provide maximum age constraints for the surface rupture that opened the paleofissure. The internal concordance of these ages suggests that they were derived from a common source, presumably the pre-earthquake topsoil at

the time; if so, they may approximate the age of the fissure-forming paleoearthquake ([Figure 10D](#)). This event (2296–1871 cal. yrs B.P.) does not necessarily immediately precede the sequence of four paleoearthquakes that we identified in the trenches <1 km to the east; however, because the ages are older than E4, we here refer to this event ‘E5’, with the acknowledgement that there may be one or more unrecognised (and unnamed) events intervening between E4 and E5. By adding these three  $^{14}\text{C}$  ages to the previously described age model as another ‘virtual’ trench, we derive an expanded, alternative model based on 19 total radiocarbon samples. This model embraces (a minimum of) six ruptures of the Kekerengu Fault including the 2016 earthquake, and nominally produces a mean (maximum) RI of  $433 \pm 22$  yrs ( $1\sigma$ ).

## **Discussion**

### ***Comparison of Kekerengu fault paleoseismicity to other paleoseismic records of faults in the marlborough fault system***

The Kekerengu Fault is one of the fastest slipping faults in the New Zealand plate boundary zone. The updated paleoseismic chronology presented in this study constrains the timing of that last 5–6 earthquakes on coastal section of the fault. Underpinned by 19 radiocarbon samples across several trenches located within a small area, this robust earthquake chronology for the eastern Kekerengu Fault makes it one of the best constrained late Holocene paleoseismic records for an active fault in the Marlborough Fault System (MFS).

The main source of slip onto the Kekerengu Fault appears to be transferred (indirectly) from the Hope Fault to the southwest – through the Jordan Thrust system and allied strands, such as the Kowhai Fault ([Figure 1](#)) ([Van Dissen and Yeats 1991](#); [Langridge et al. 2003](#); [Langridge et al. 2013](#); [Khajavi et al. 2016](#)). The Hope Fault has the highest slip rate of the four primary faults in the MFS, at  $23 \pm 4$  mm/yr ([Langridge et al. 2013](#)), taking up the majority of slip from the Alpine Fault. A compilation of paleoseismic data for the faults in the MFS is presented in [Hattem et al. \(2019\)](#), including data for the Hurunui section of the Hope Fault ([Langridge et al. 2013](#); [Khajavi et al. 2016](#)), the Conway section of the Hope Fault ([Langridge et al. 2003](#); [Hattem et al. 2019](#)), and also the Alpine Fault ([Wells et al. 1999](#); [Howarth et al. 2018](#)). This compilation also includes paleoseismic data for the Wairarapa Fault in the North Island of New Zealand ([Little et al. 2009](#)), and to it we have added our revised earthquake chronology data for surface rupturing on the Kekerengu Fault (shaded green, [Figure 11](#)), as well as recent paleoseismic data from Lake Grassmere, located in

the transition zone between the Hikurangi subduction zone and the MFS (Pizer et al. 2021, shaded blue on Figure 11).

The pink horizontal bands on Figure 11 represent potential past cases of clustered (<100 yr interval) events, suggestive of ‘en masse strain release’, or many earthquakes possibly happening in a short time frame (Hattem et al. 2019). These are time periods in which most (or all) of the major faults in the MFS experienced surface ruptures of a similar (statistically overlapping) age. The last four paleoearthquakes on the Kekerengu Fault (E1-E4) overlap with others on the Hope and Alpine faults, suggesting that the Kekerengu Fault may often rupture in close sequence (or synchronously) with other major faults. The Kekerengu Fault does not appear to have ruptured ‘alone’ in the last ~2000 years, however, the imprecision in the dating, coupled with the short recurrence time (~300-500 yrs) of adjacent faults (Alpine, Hope, and Kekerengu), make robust differentiation of individual events impossible. We note that oldest event that we document for the Kekerengu Fault (paleofissure opening, E5; labelled KE5 in Figure 11) seems to overlap in age with the oldest events from both Lake Grassmere and the Wairarapa Fault (LG2 and CC3 on Figure 11, respectively), suggesting a new and older potential clustered event than was established by Hattem et al. (2019).

The Papatea Fault also intersects the Kekerengu Fault (Figure 1). The Papatea Fault slips sinistrally and with reverse motion, raising an uplifted block between the Hope Fault and the Jordan Thrust (Langridge et al. 2018). Prior to the Kaikōura earthquake, the Papatea Fault was not recognised as active, but results of recent trenching on that fault (Langridge *et al.*, this issue), suggest that some of its late Holocene surface ruptures may overlap in time with those that we have here established for the Kekerengu Fault.

While this compilation of MFS paleoseismic records is comprehensive (Figure 11), it also shows that at present, the detail of our fault records, as well as current dating precision, does not allow us to conclusively identify multi-fault ruptures in the paleoseismic record. Although the clusters of events on Figure 11 may be explained by possible occurrences of multi-fault rupture, we cannot rule out earthquake triggering as an explanation for these clusters. Additionally, some events in the record do not appear to be temporally related to events on other faults in the MFS (e.g. GB4), suggesting that some ruptures may be isolated (Hattem et al. 2019). These variable records suggest that to fully understand seismic hazard in the region, allowances must be made in seismic hazard models for various rupture scenarios in which different combinations of faults rupture together, and on their own (see also Brough et al. 2021).

### Implications for future paleoseismic studies

Potential insight into trench-based paleoseismic interpretation is provided by our re-excavation of a paleoseismic trench that was displaced by ~9 m during a large strike-slip earthquake. The post-earthquake 2018 trench logs (Figures 6–8) show that after the large, 2016 surface rupture an overprint of new deformation (some of it distributed) caused subtle changes in stratigraphic or structural relationships indicative of past earthquakes, such as angular unconformities, upward fault truncations, and infilled fissures. Most (but not all) of the key pre-2016 relationships, however, were still discernible in the stratigraphic record. This was true despite the subtle nature of many of these relationships in fault-perpendicular view (e.g. dip separations on individual fault strands of only a few cm), and despite the large slip and deformation associated with the last rupture. In some cases, after the 2016 earthquake we uncovered new evidence for previously identified paleoearthquakes on the exhumed trench walls, and on their extensions into previously unexcavated ground—evidence that had not been documented prior to the 2016 earthquake. The ‘new’ evidence was observed in part because of the large out-of-plane motion (including distributed shearing) that took place in 2016. This process locally carried previously unseen features into the plane of view of the re-excavated trench wall.

Of course, in some parts of the 2016 rupture zone small stratigraphic units, faults, and other features that had existed prior to 2016 were destroyed: for example, in the central rupture zones flanking faults 1 and 4 (Figures 6 and 8). Both fault 1 and 4 existed prior to 2016, but they terminated upward against unfaulted beds (i.e. they were ‘blind’). Their reactivation in 2016 destroyed the upward terminations as the faults propagated all the way up to the modern ground surface. Other nearby fault strands (e.g. faults 3 and 5 in Figures 3 and 6) were not reactivated and their upward terminations remained; however, the overprint of distributed deformation in 2016 changed the dips of the faults and bedding, altering the geometry of their intersection.

Our ‘before’ and ‘after’ comparison shows that a large earthquake can produce cross-cutting relationships between different fault strands active during the same earthquake. In the future, a paleoseismologist might incorrectly interpret these fault intersections as being indicative of more than one surface rupturing event. For example, on the NE wall of trench T1S, the gently dipping, upper part of fault 1 emplaces a large bulge (moletrack) of backfill material (unit *tbf*) outwardly to the northwest over older peaty units (Figure 7). Internally, this thrust-like bulge is complexly imbricated, and it contains multiple, cross-

cutting fault strands. All these faults formed in different (likely co-seismic) stages of the 2016 earthquake, over a period of just a few seconds. Another example of these cross-cutting fault strands is on the SW wall of trench T1N, where fault 1 splits into two strands, labelled 1A and 1B (Figure 8). Sample N1-01 from this trench wall (unit *bp*) yielded a modern radiocarbon age, leading us to infer that this fault ruptured in 2016 in at least two stages; first, a small fissure opened at the ground surface and was filled in by material that already lay on the ground surface (units *bsc*, *bp* and *usc*). Very shortly afterward, this fissure was overridden by a fault (1B) that displaced units *o*, *ml* and *psp* overtop of the fissure and sealed it (Morris et al. 2021). Again, this demonstrates that large rupture events may be difficult to interpret in trenches, and could lead to misinterpretation of and/or contradictions within paleoseismic data and sequences.

Our post-2016 excavations allowed us to carry out a ‘test’ on trench-based dating of a large-slip strike-slip earthquake of known age. While there was no post-earthquake, unfaulted layer that we could date to provide a maximum age bracket for the earthquake, we did date four samples of near-surface faulted material that a paleoseismologist may interpret as providing maximum ages for the 2016 event, and probably only just slightly older. Three of these returned modern radiocarbon ages, but it is worth noting that one did not. Sample S1-03 taken from a faulted wedge of organic clay (unit *fp*, Figure 6) returned an age of 632–533 cal. yrs B.P.—much older than modern. We interpret this anomalously old age as indicating that the fault wedge was derived from the *lp* unit, and that it had been laterally introduced into the plane of the trench from the southwest, and also pushed upward to reach the modern ground surface. Finally, we observed that deep, open fissures that formed in the 2016 earthquake were almost completely filled in within two years, in large part by the downward toppling, falling, and redeposition of pre 2016 soil and colluvium. This leads us to a further methodological conclusion—that in many cases,  $^{14}\text{C}$  ages of detrital material in the infill of coseismic fissures will provide a maximum age constraint for the earthquake—not a minimum one.

## Conclusion

Following the 2016 earthquake, the re-excavation and extension of both halves of a displaced paleoseismic trench, and the excavation of a new trench nearby provided an opportunity to reinforce and refine the known established paleoseismic sequence for the Kekerengu Fault. Our revised paleoearthquake chronology is based on OxCal modelling of an ordered sequence of 19 radiocarbon samples (some of them

aggregated into internally un-ordered ‘phases’), sixteen of them taken from the walls of four pre- to post-earthquake trenches, and three from a nearby paleofissure deposit. These ages provide robust age constraints for six late Holocene surface ruptures near the Marlborough coast—two more than were reported by Little et al. (2018). Based on the last five events (E0 to E4), our new analysis yields an updated estimate for the mean recurrence interval of  $375 \pm 32$  yrs ( $1\sigma$ ) for the Kekerengu Fault since  $\sim 1650$  cal. B.P.

The three samples of charcoal infilling the paleofissure provided information about a fifth and older paleo-event on the fault; this oldest dated event (E5) may not have immediately preceded E4, but is incorporated into an alternative model for earthquakes on the fault based on an assumption that all events up to the time of E5 have been recognised. This alternative age model yields a mean recurrence interval estimate of  $433 \pm 22$  yrs ( $1\sigma$ ). This represents a maximum estimate of the mean RI, as there may be undocumented events between E4 and E5.

While comparisons of regional paleoseismic records may be useful in understanding local seismic hazard, the current compilation of MFS fault rupture histories shows that greater dating precision is needed if we wish to a) conclusively identify multi-fault ruptures in the earthquake record, and b) better understand the breadth of possible rupture scenarios in a the region.

Our ability to compare structural data from before and after the 2016 earthquake (Morris et al. 2021) combined with detailed stratigraphic and chronologic information (this paper) shows that a large earthquake can produce cross-cutting relationships between different fault strands active during the same earthquake, which should be considered by paleoseismologists in the future, particularly when interpreting the structural record of faults with known large event displacements.

Finally, after observing that most of the fissures formed in 2016 were infilled in  $\sim 2$  years with pre-2016 soil and/or colluvium, we conclude that in many cases,  $^{14}\text{C}$  ages of coseismic fissure infill will provide a maximum age constraint for the fissure-opening earthquake.

## Acknowledgements

Thanks are extended to the EQC (grant 18-758) for funding this research project. We also thank Emma Watson and Lynda Petherick for their help in the trenching expedition of February 2018, and Rob Langridge and Carolyn Boulton for their reviews of an earlier manuscript.

## Data availability statement

The supplemental files cited in this paper along with any other data that support the findings of this study are openly

available in figshare at <https://doi.org/10.6084/m9.figshare.19407587.v1>.

## Disclosure statement

No potential conflict of interest was reported by the author(s).

## Funding

This work was supported by Earthquake Commission [grant number 18/758].

## ORCID

Philippa Morris  <http://orcid.org/0000-0001-7720-2012>

Timothy Little  <http://orcid.org/0000-0002-5783-6429>

Matthew Hill  <http://orcid.org/0000-0002-1818-1458>

Jessie Vermeer  <http://orcid.org/0000-0001-8349-0137>

Kevin Norton  <http://orcid.org/0000-0002-7995-6464>

## References

- Barnes PM, Pondard N, Lamarche G, Mountjoy J, Van Dissen R, Litchfield N. 2008. It's our fault: Active faults and earthquake sources in Cook Strait, National Institute of Water & Atmospheric Research (NIWA) Client Report WLG2008-56.
- Bronk Ramsey C. 2008. Deposition models for chronological records. *Quaternary Science Reviews*. 27(1-2):42-60.
- Brough T, Nicol A, Stahl T, Pettinga JR, Dissen RV, Clark D, Khajavi N, Pedley K, Langridge R, Wang N. 2021. Paleoseismicity of the western Humps fault on the Emu Plain, North Canterbury, New Zealand. *New Zealand Journal of Geology and Geophysics*. 65(2):1-14.
- Hamling IJ, Hreinsdóttir S, Clark K, Elliott J, Liang C, Fielding E, Litchfield N, Villamor P, Wallace L, Wright TJ, D'Anastasio E. 2017. Complex multifault rupture during the 2016 M w 7.8 Kaikōura earthquake, New Zealand. *Science*. 356(6334):p.eaam7194.
- Hatem AE, Dolan JF, Zinke RW, Langridge RM, McGuire CP, Rhodes EJ, Brown N, Van Dissen RJ. 2020. Holocene to latest Pleistocene incremental slip rates from the east-central Hope fault (Conway segment) at Hossack Station, Marlborough fault system, South Island, New Zealand: Towards a dated path of earthquake slip along a plate boundary fault. *Geosphere*. 16(6):1558-1584.
- Hatem AE, Dolan JF, Zinke RW, Van Dissen RJ, McGuire CM, Rhodes EJ. 2019. A 2000 yr paleoearthquake record along the Conway segment of the Hope fault: Implications for patterns of earthquake occurrence in northern South Island and southern North Island, New Zealand. *Bulletin of the Seismological Society of America*. 109(6):2216-2239.
- Hill MP, Ashraf S. 2017. Digital surface models from Clarence to Kekerengu using semi-global matching and structure from motion photogrammetry and their use in geomorphic interpretation. *GNS Science Report*, 17, GNS Science, Lower Hutt, New Zealand.
- Hogg A, Hua Q, Blackwell P, Niu M, Beck C, Guilderson T, Heaton T, Palmer J, Reimer P, Reimer R, Turney C, et al. 2013. SHCal13 Southern Hemisphere Calibration, 0-50,000 years cal. B.P. *Radiocarbon*. 55:1189-1903.
- Howarth JD, Cochran UA, Langridge RM, Clark K, Fitzsimons SJ, Berryman K, Villamor P, Strong DT. 2018. Past large earthquakes on the Alpine Fault: paleoseismological progress and future directions. *New Zealand Journal of Geology and Geophysics*. 61(3):309-328.
- Kearse J, Little TA, Van Dissen RJ, Barnes PM, Langridge R, Mountjoy J, Ries W, Villamor P, Clark KJ, Benson A, Lamarche G. 2018. Onshore to Offshore Ground-Surface and Seabed Rupture of the Jordan-Kekerengu-Needles Fault Network during the 2016 Mw 7.8 Kaikōura Earthquake, New Zealand Onshore to Offshore Ground-Surface and Seabed Rupture of the Jordan-Kekerengu-Needles Fault Network. *Bulletin of the Seismological Society of America*. 108(3B):1573-1595.
- Khajavi N, Langridge RM, Quigley MC, Smart C, Rezanejad A, Martín-González F. 2016. Late Holocene rupture behavior and earthquake chronology on the Hope fault, New Zealand. *Bulletin*. 128(11-12):1736-1761.
- Langridge R, Campbell J, Hill N, Pere V, Pope J, Pettinga J, Estrada B, Berryman K. 2003. Paleoseismology and slip rate of the Conway Segment of the Hope Fault at Greenburn Stream, South Island, New Zealand. *Annals of Geophysics*. 46(5). <https://doi.org/10.4401/ag-3449>.
- Langridge RM, Almond PC, Duncan RP. 2013. Timing of late Holocene paleoearthquakes on the Hurunui segment of the Hope fault: Implications for plate boundary strain release through South Island, New Zealand. *Bulletin*. 125(5-6):756-775.
- Langridge RM, Rowland J, Villamor P, Mountjoy J, Townsend DB, Nissen E, Madugo C, Ries WF, Gasston C, Canva A, Hatem AE. 2018. Coseismic rupture and preliminary slip estimates for the Papatea fault and its role in the 2016 M w 7.8 Kaikōura, New Zealand, Earthquake. *Bulletin of the Seismological Society of America*. 108(3B):1596-1622.
- Lienkaemper JJ, Bronk Ramsey C. 2009. OxCal: Versatile tool for developing paleoearthquake chronologies—A primer. *Seismological Research Letters*. 80(3):431-434.
- Litchfield NJ, Villamor P, Dissen RJV, Nicol A, Barnes PM, Barrell DJA, Pettinga JR, Langridge RM, Little TA, Mountjoy JJ, Ries WF. 2018. Surface rupture of multiple crustal faults in the 2016 M w 7.8 Kaikōura, New Zealand, Earthquake. *Bulletin of the Seismological Society of America*. 108(3B):1496-1520.
- Little T, Jones A. 1998. Seven million years of strike-slip and related off-fault deformation, northeastern Marlborough fault system, South Island, New Zealand. *Tectonics*. 17(2):285-302.
- Little VDR, Kearse J, Norton K, Benson A, Wang N. 2018. Kekerengu fault, New Zealand: Timing and size of Late Holocene surface ruptures. *Bulletin of the Seismological Society of America*. 108(3B):1556-1572.
- Little TA, Morris P, Hill MP, Kearse J, Van Dissen RJ, Manousakis J, Zekkos D, Howell A. 2021. Coseismic deformation of the ground during large-slip strike-slip ruptures: Finite evolution of "mole tracks". *Geosphere*. 17(4):1170-1192.
- Little VDR, Schermer E, Carne R. 2009. Late Holocene surface ruptures on the southern Wairarapa fault, New Zealand: Link between earthquakes and the uplifting of beach ridges on a rocky coast. *Lithosphere*. 1(1):4-28.
- Morris P, Little T, Van Dissen R, Hill M, Hemphill-Haley M, Kearse J, Norton K. 2021. Evaluating 9 m of near-surface transpressional displacement during the Mw 7.8 2016 Kaikōura earthquake: re-excavation of a pre-earthquake paleoseismic trench, Kekerengu Fault, New Zealand. *New Zealand Journal of Geology and Geophysics*. 65(2):1-19.

- Mouslopoulou V, Saltogianni V, Nicol A, Oncken O, Begg J, Babeyko A, Cesca S, Moreno M. 2019. Breaking a subduction-termination from top to bottom: the large 2016 Kaikōura Earthquake, New Zealand. *Earth and Planetary Science Letters*. 506:221–230.
- Nicol A, Khajavi N, Pettinga JR, Fenton C, Stahl T, Bannister S, Pedley K, Hyland-Brook N, Bushell T, Hamling I, Ristau J. 2018. Preliminary geometry, displacement, and kinematics of fault ruptures in the epicentral region of the 2016  $M_w$  7.8 Kaikōura, New Zealand, earthquake. *Bulletin of the Seismological Society of America*. 108(3B):1521–1539.
- Pizer C, Clark K, Howarth J, Garrett E, Wang X, Rhoades D, Woodroffe S. 2021. Paleotsunamis on the Southern Hikurangi Subduction Zone, New Zealand, Show Regular Recurrence of Large Subduction Earthquakes. *The Seismic Record*. 1(2):75–84.
- Stuiver M, Polach HA. 1977. Discussion: reporting of  $^{14}C$  data. *Radiocarbon*. 19:355–363.
- Van Dissen R, Yeats RS. 1991. Hope fault, Jordan thrust, and uplift of the seaward Kaikōura Range, New Zealand. *Geology*. 19(4):393–396.
- Wells A, Yetton MD, Duncan RP, Stewart GH. 1999. Prehistoric dates of the most recent Alpine fault earthquakes, New Zealand. *Geology*. 27(11):995–998.
- Zekkos D. 2018, June. Structure-from-Motion based 3D mapping of landslides & fault rupture sites during 2016 Kaikoura earthquake reconnaissance. In 11th US National Conference on Earthquake Engineering.